AD-A114 160 OPTIMETRICS INC ANN ARBOR MI F/G 4/1
LASER PROPAGATION RESEARCH. VOLUME I. SLANT PATH TRANSMISSION M--ETC(U)
NOV 80 W M GUTMAN, S T HANLEY DAAD07-80-C-0056
UNCLASSIFIED OMI-80-008-VOL-1 NL

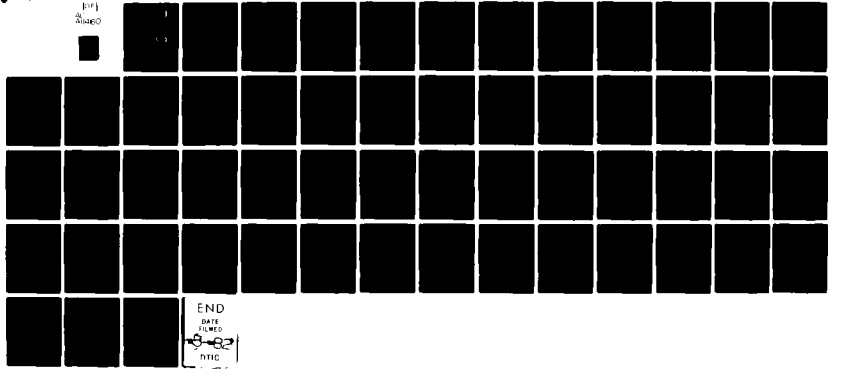

END
DATE FILMED
DTIC

PHOTOGRAPH THIS SHEET

AD-A114 160

DTIC ACCESSION NUMBER

11

LEVEL

[redacted]

INVENTORY

Laser Propagation Research. Volume I

DOCUMENT IDENTIFICATION Rept. No. OMI-80-008(I)

Contract DAAD07-80-C-0056 Nov. 80

DISTRIBUTION STATEMENT A

Approved for public release;
Distribution Unlimited

DISTRIBUTION STATEMENT

ACCESSION FOR	
NTIS GRA&I	☒
DTIC TAB	☐
UNANNOUNCED	☐
JUSTIFICATION	
BY Per Ltr. on File	
DISTRIBUTION /	
AVAILABILITY CODES	
DIST	AVAIL AND/OR SPECIAL
A	

DISTRIBUTION STAMP

DTIC COPY INSPECTED 2

DTIC
ELECTE
S MAY 6 1982 D
D

DATE ACCESSIONED

DATE RECEIVED IN DTIC

PHOTOGRAPH THIS SHEET AND RETURN TO DTIC-DDA-2

DTIC FORM OCT 79 70A

DOCUMENT PROCESSING SHEET

OMI-80-008(I)

LASER PROPAGATION RESEARCH

VOLUME I
SLANT PATH TRANSMISSION MEASUREMENTS

William M. Gutman
Stephen T. Hanley

Prepared for

Atmospheric Sciences Laboratory
White Sands Missile Range, New Mexico

Contract DAAD07-80-C-0056

November 1980

OptiMetrics, Inc.
2000 Hogback Rd., Suite 3
Ann Arbor, MI 48104

UNCLASSIFIED

SECURITY CLASSIFICATION OF THIS PAGE *(When Data Entered)*

REPORT DOCUMENTATION PAGE	READ INSTRUCTIONS BEFORE COMPLETING FORM
1 REPORT NUMBER	2 GOVT ACCESSION NO: AD-A114 160 — 3 RECIPIENT'S CATALOG NUMBER
4 TITLE *(and Subtitle)*: LASER PROPAGATION RESEARCH VOLUME I SLANT PATH TRANSMISSION MEASUREMENTS	5 TYPE OF REPORT & PERIOD COVERED: Technical Report 3/80 - 10/80 6 PERFORMING ORG REPORT NUMBER: OMI-80-008(I)
7 AUTHOR*(s)*: William M. Gutman Stephan T. Hanley	8 CONTRACT OR GRANT NUMBER*(s)*: DAAD07-80-C-0056
9 PERFORMING ORGANIZATION NAME AND ADDRESS: OptiMetrics, Inc. 2000 Hogback Road, Suite 3	10 PROGRAM ELEMENT, PROJECT, TASK AREA & WORK UNIT NUMBERS: Volume I Task F.3.2
11 CONTROLLING OFFICE NAME AND ADDRESS: Atmospheric Sciences Laboratory US Army Electronics R&D Command WSMR, NM 88002	12 REPORT DATE: November 1980 13 NUMBER OF PAGES: 50
14 MONITORING AGENCY NAME AND ADDRESS *(if different from Controlling Office)*	15 SECURITY CLASS *(of this report)*: Unclassified 15a DECLASSIFICATION/DOWNGRADING SCHEDULE

16 DISTRIBUTION STATEMENT *(of this Report)*

DISTRIBUTION STATEMENT A
Approved for public release;
Distribution Unlimited

17 DISTRIBUTION STATEMENT *(of the abstract entered in Block 20, if different from Report)*

18 SUPPLEMENTARY NOTES

19 KEY WORDS *(Continue on reverse side if necessary and identify by block number)*

High Energy Laser
Atmospheric Transmission
ARKY Site
NOP Site
H_2O, HDO, N_2O, O_3, THC, CH_4
Fourier Transform Spectrometer (FTS)
Solar Spectrum

20 ABSTRACT *(Continue on reverse side if necessary and identify by block number)*

An existing Fourier Transform Spectrometer (FTS) data base of slant path atmospheric transmission spectra using the sun as a source is described. Recent improvements to the FTS measurements system are discussed and results of pyroelectric radiometer measurements of slant path solar transmission are reviewed.

Slant path atmospheric transmission modeling developments and use of these models in the interpretation of slant path FTS transmission data are discussed.

DD FORM 1 JAN 73 1473 EDITION OF 1 NOV 65 IS OBSOLETE

UNCLASSIFIED

SECURITY CLASSIFICATION OF THIS PAGE *(When Data Entered)*

Techniques for atmospheric absorbing gas vertical density profile extraction are presented and results of model comparisons with FTS data are reviewed.

Recent measurements of H_2O, N_2O, THC, CH_4, O_3, and CO_2 atmospheric concentrations at the ARKY and NOP sites at WSMR are presented and discussed. Results of aerosol particulate distribution and mass loading measurements at the WSMR-NOP sites are presented and described.

CONTENTS

LIST OF ILLUSTRATIONS

1
INTRODUCTION

This report describes work performed for the Atmospheric Sciences Laboratory (ASL) in support of their High Energy Laser Meteorology (HELMET) responsibility to the High Energy Laser Systems Test Facility (HELSTF). The measurements and analyses reported herein continue and extend work begun in 1977. It describes work completed during the period 1 March through 30 September 1980.

In the interest of clarity, this report has been separated into two volumes. Volume 1 describes progress, results, and data analyses associated with the measurements at atmospheric transmission spectra using the sun as a source. Volume II describes recent work carried out in atmospheric gas analysis studies and contains results of measurements performed during the most recent reporting period. This volume is devoted to the FTS Solar Measurements.

2
SOLAR SPECTRAL MEASUREMENTS

2.1 AUGMENTATION OF EXISTING FOURIER TRANSFORM SPECTROMETER DATA BASE

The techniques and procedures used in the accumulation of the data base consisting of sets of solar source atmospheric spectra, and the extraction of extinction coefficients from these spectra has been reported previously [1,2,3] and will not be discussed in great detail. Measurements were made on twelve days in the first quarter of the reporting period using the original software as supplied by the Fourier Transform Spectrometer (FTS) manufacturer (MIDAC Corporation). In the final quarter, trial measurements were made on three additional days using improved operating software supplied by MIDAC. These measurements were made primarily as a test of the usefulness of the new system, but the results are available. Since a total of only 15 days of measurements were made during the present reporting period, and since these days are not necessarily representative of each seasonal period, average extinction coefficients are not very meaningful except when viewed in the context of the entire 2-1/2 year data base. For this reason, tabulations and plots of these values are not presented in this report.

2.2 INVESTIGATION OF THE USE OF PYROELECTRIC RADIOMETERS FOR SOLAR SPECTRAL MEASUREMENTS

During several of the FTS data runs, two Laser Precision Corporation electrically calibrated pyroelectric radiometers were operated simultaneously with the Fourier Transform Spectrometer. These devices were provided by the Air Force Weapons Laboratory, and were operated in the same

beam of solar radiation as the spectrometer. Each was equipped with a narrow bandpass filter with a transmission width of about 10 cm^{-1} centered at about 2585 cm^{-1}. This is within the DF laser region of the spectrum. The majority of the spectra collected with the Fourier Transform Spectrometer were collected at a nominal resolution of 0.12 cm^{-1}. This value represents the spacing between the first order zero crossings of the unapodized sin x/x instrumental line shape. Comparing a given data point in several spectra, the values are proportional to the energy within the resolution element falling on the detector during the scan. A plot of the log of this value versus airmass yields the extinctance which is the slope of this graph. The technique is discussed fully in References 1 and 2. It had been hoped that the 10 cm^{-1} bandpass filter would be narrow enough that a similar technique applied to the radiometer data would yield average extinction coefficients over the spectral region which would correlate with those obtained at high resolution with the spectrometer. It would then have been possible to monitor variations in extinction values with much simpler and less expensive instrumentation.

The pyroelectric devices proved not to be practical for such use, however. They exhibit a long term radiometric equivalent drift on the order of 2 microwatts. The solar flux transmitted through the bandpass filter however, is on the order of only a few microwatts. The radiometer response is sampled at the rate of about 3 Hz. Figure 1 is a plot of the log of the relative energy falling on the pyroelectric detectors during one sampling interval as a function of air mass for each of the two radiometers for a typical day. Included for comparison is a typical plot taken from 0.12 cm^{-1} resolution Fourier transform spectra for the DF laser line $P_3(6)$ frequency of 2594.20 cm^{-1}.

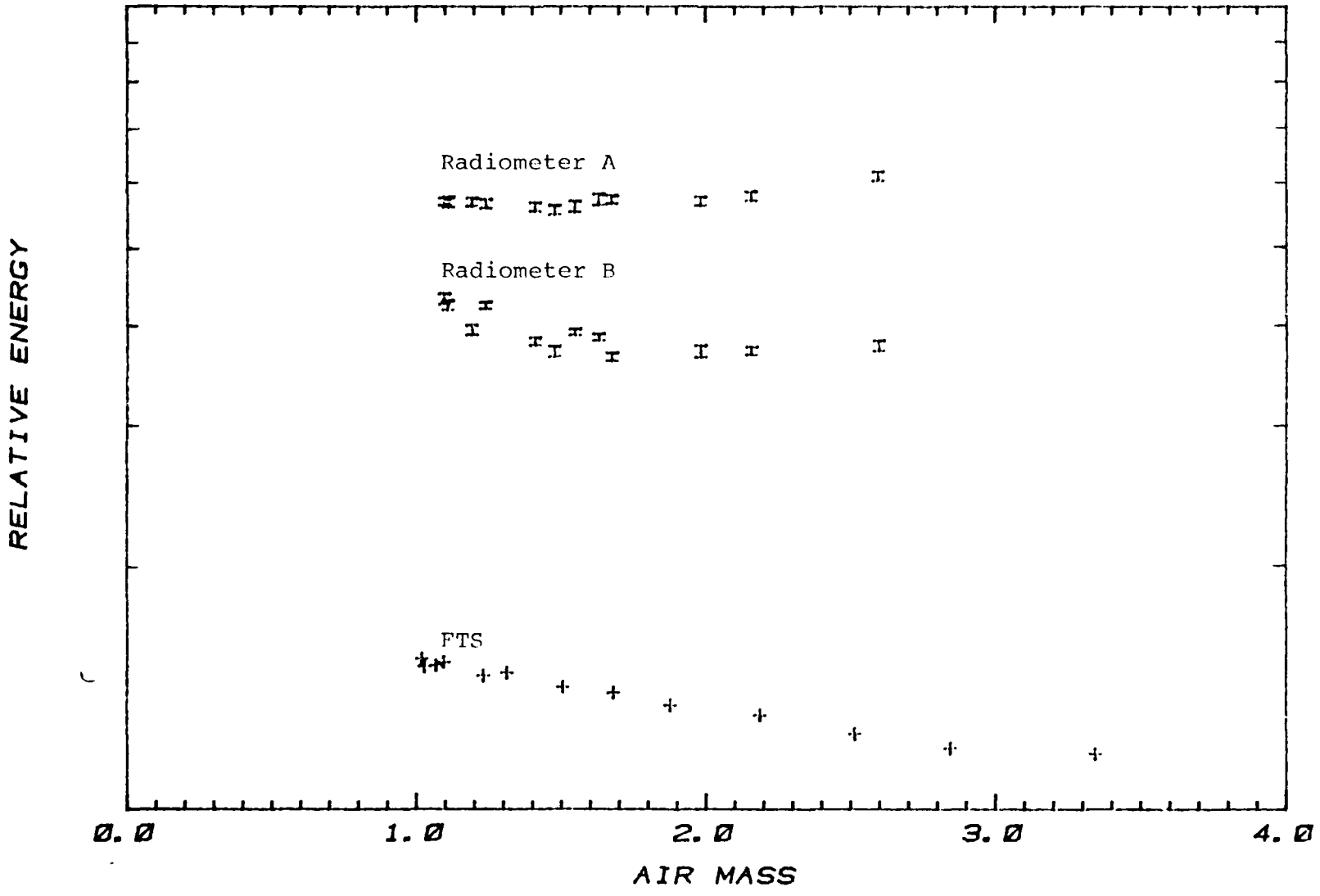

FIGURE 1. RELATIVE ENERGY RECEIVED BY THE DETECTOR DURING A SAMPLING INTERVAL IS PLOTTED SEMI-LOGARITHMICALLY VERSUS AIR MASS FOR THE TWO PYROELECTRIC RADIOMETERS, AND FOR THE FTS SPECTRA AT DF LASER LINE $P_3(6)$ FREQUENCY AT 2594.20 cm^{-1}. THE SLOPES OF THE CURVES ARE PROPORTIONAL TO THE EXTINCTION COEFFICIENT.

The extent of the error bars represents the maximum and minimum values observed during a 15-second time period. It is clear that a least squares fit to these data would exhibit a large standard deviation, and that the slopes are not consistent with each other. In fact, in one case, the energy decreases with decreasing air mass. It is thus apparent that the electrically calibrated radiometers are not useful for making measurements with such a narrow bandpass filter. In order to reduce the drift problem, the energy falling on the detector should be large compared with the drift, and this could be achieved by using a much wider bandpass. Such a measurement, however, which would involve a region containing perhaps several dozen strong spectral lines, would bear little relation with the high resolution spectral measurements.

2.3 ADDITIONAL INSTRUMENTAL CAPABILITIES

2.3.1 IMPLEMENTATION OF IMPROVED FTS SOFTWARE

A major part of the FY 1980 effort was devoted to the implementation of the improved MIDAC Corporation software for the spectrometer system. The primary motivation for the acquisition of the software update was to be able to perform Fourier transforms on larger data sets. The previous system was limited to transforms of 131072 points, and in order to eliminate aliasing problems, this constraint effectively limited the resolution to 0.12 cm^{-1}, where the resolution criterion is the spacing between the first order zero crossings of the unapodized sin x/x instrument lineshape. This resolution proved to be insufficient to answer subtle questions about the shapes of atmospheric CO_2 absorption lines.

MIDAC Corporation chose to completely revise its spectrometer operating software. The foremost improvement was the

doubling of the size of the data set which could be transformed. This of course doubled the resolution which could be used without aliasing problems. Another significant improvement was the utilization of the stepped gain feature. This feature, which had always been available in hardware, was made accessible from software. In effect, after a specified number of data points, the overall interferogram signal gain before digitization is increased by a factor of 8. The step is made between data points, and at a location in the interferogram sufficiently past the center burst where the dynamic range of the signal is much smaller. The net effect is improved utilization of the analog-to-digital converter and improved signal to noise ratio. Another important improvement entailed full use of a file header containing all pertinent information about each spectrum. Included in this information is the bit shift applied to each interferogram before transformation. This shift is applied to eliminate some noise bits prior to transformation, and in effect scales the resulting spectrum by powers of two. Having this information available allows the direct comparison of spectra without having to surmise the relative scaling as was necessary under the old operating system. Finally, the new MIDAC software is much simpler to use for the operator. The desired spectrometer operating conditions are entered directly into a control file by the operator rather than by coding in the form of control words. The net result is that the system can, in principle, be fully utilized by an operator with little training in minicomputers and the intricacies of the hardware.

Of course these improvements were not made without some sacrifices. Under the previous system, the interferograms were collected into double 16-bit integers, and the spectra resulting were in the form of single 16-bit integers. In order to eliminate the resulting file size discrepancy,

and to increase the dynamic range available in the spectra, the new system uses double words for the spectra as well as the interferograms. This fact coupled with doubling the size of the data sets in order to double the resolution reduces the number of spectra which can be stored on a removable disc cartridge to two, a number insufficient for calculation of extinction coefficients. In addition, the time required for the Fourier transformation of a 262144 point data set is much longer, due both to its size and to the fact that the operation is done in double precision. Rather than having the capability to collect and transform four spectra per hour as before, the limit was about one per hour. MIDAC was able to overcome the storage and time limitations through the use of the magnetic tape drive. A modified version of the software was provided which can be used to store each complete interferogram on a reel of magnetic tape as it is collected. A 10-inch reel of tape can contain eleven high resolution data sets. After a reel of tape is filled with interferograms, each file can be read from the tape by the data system, Fourier transformed, and the spectrum written back onto the tape over the interferogram. This can be accomplished after all data collection is complete, and hence transformation does not place time constraints on data collection.

The data tapes which result from the procedure described above are of course incompatible with those which were created using the old operating software, so it was necessary to modify all previously implemented data reduction programs used with the HP-1000 system. The double word integers could not be read directly, so it was necessary to construct a routine to read the two words separately, but properly recover the double word value. It was found that the values could be converted to two word real numbers

in the Hewlett-Packard format without loss of precision. The previously used tape read subroutine was modified in this manner. The point spacing in the spectra, of course, was also different. For archival storage, a further refinement was made. The MIDAC software created tapes consist of 512 word or 256 data point records on 800 bpi 9-track tapes. By writing a new tape consisting of 8192 word or 4096 point records, most of the space required for inter-record gaps could be saved. Furthermore, it is possible to save only those spectral regions of interest, and since the new tape is written on a 1600 bpi tape drive, the net result is that several days of spectra can be stored on a given tape. New versions of the data reduction tapes were then written so that these archival tapes can be used directly in the procedure.

Some difficulties were encountered with the new MIDAC software, initially. The ASL spectrometer system utilizes a Versatec plotter/printer for spectral plotting which is different from that in the MIDAC test system. Several iterations were required in the plotting routine to correctly interface with the device, and to produce plots with a correct frequency scale. After the problems were overcome, the system was tested by obtaining spectra on three days, and calculating extinction values in the usual manner. When a workable routine had been devised, and the system was operating properly, the decision was made to move the spectrometer into its van.

2.3.2 INSTALLATION OF THE FTS SYSTEM IN THE FIELD MEASUREMENT VAN

The van to be used for field measurements had been previously prepared prior to the FTS system installation. Every effort was made to insure a weather tight and dust

free environment for the system. The roof was repaired, the floor tiled, the walls lined, and the exterior painted with a highly reflective white paint to minimize the summertime thermal load. However, due to uncontrollable circumstances during the move, the germanium on potassium bromide beam-splitter which had been used during the collection of all previous solar spectra was damaged. A replacement was ordered, and was being installed and tested as the reporting period ended. In the van, the system will be used to collect slant path solar spectra in much the same way as has been done previously. A Carson Astronomical Instruments 6-inch heliostat is available for solar tracking. However, this device required minor modification for proper operation. The tracking system contains a drive motor for the right ascension axis and slew motors for both the right ascension and declination axes. When the right ascension drive motor was in operation, the slew motor, which should have remained fixed, tended to rotate with the net result that the tracking mirror remained fixed. After numerous attempts to correct this problem by balancing the frictional forces with a crude spring clutch incorporated into the system, it became apparent that when the frictional forces were large enough to prevent the slew motor from freely rotating, then the drive motor torque was insufficient to overcome the same frictional forces. The situation was remedied by modifying the electrical circuit so that a DC voltage is applied across the slew motor whenever it is not being used to slew. A full wave rectified 85 volt rms AC voltage proved sufficient to solve the problem.

3
ANALYSIS AND INTERPRETATION OF PREVIOUSLY COLLECTED FOURIER TRANSFORM SPECTROMETER DATA

Analysis of previously collected data carried out during this reporting period can be divided into two categories: a) attempts to correlate extinction coefficient variation with variation in other measurable parameters; and b) attempts to use accepted atmospheric models to predict measured slant path transmission. Additionally, preliminary efforts to extract vertical profiles of infrared absorbing species based solely on measured slant path transmission spectra have proved successful.

3.1 CORRELATION OF CO_2 AND DF LASER LINE EXTINCTION COEFFICIENTS WITH ATMOSPHERIC ABSORPTION LINE MEASUREMENTS

A computer program was written to plot the measured extinction coefficient at any CO_2 or DF laser frequency for which FTS measurements are made as a function of the absorption coefficient measured at the peak of any of several atmospheric H_2O or HDO absorption lines. The atmospheric line extinction coefficient values are taken to be the difference between the extinction coefficient measured at line center and the value measured some distance away from line center. It is assumed that aerosol scattering and molecular continuum absorption effects are essentially constant over a few cm^{-1} and so the difference between the line center and wing extinction coefficient values represents molecular abosrption due to that line. This point is discussed more thoroughly in Reference 2. Figures 2 and 3 are plots of extinction coefficient at two different DF laser frequencies versus molecular absorption coefficient

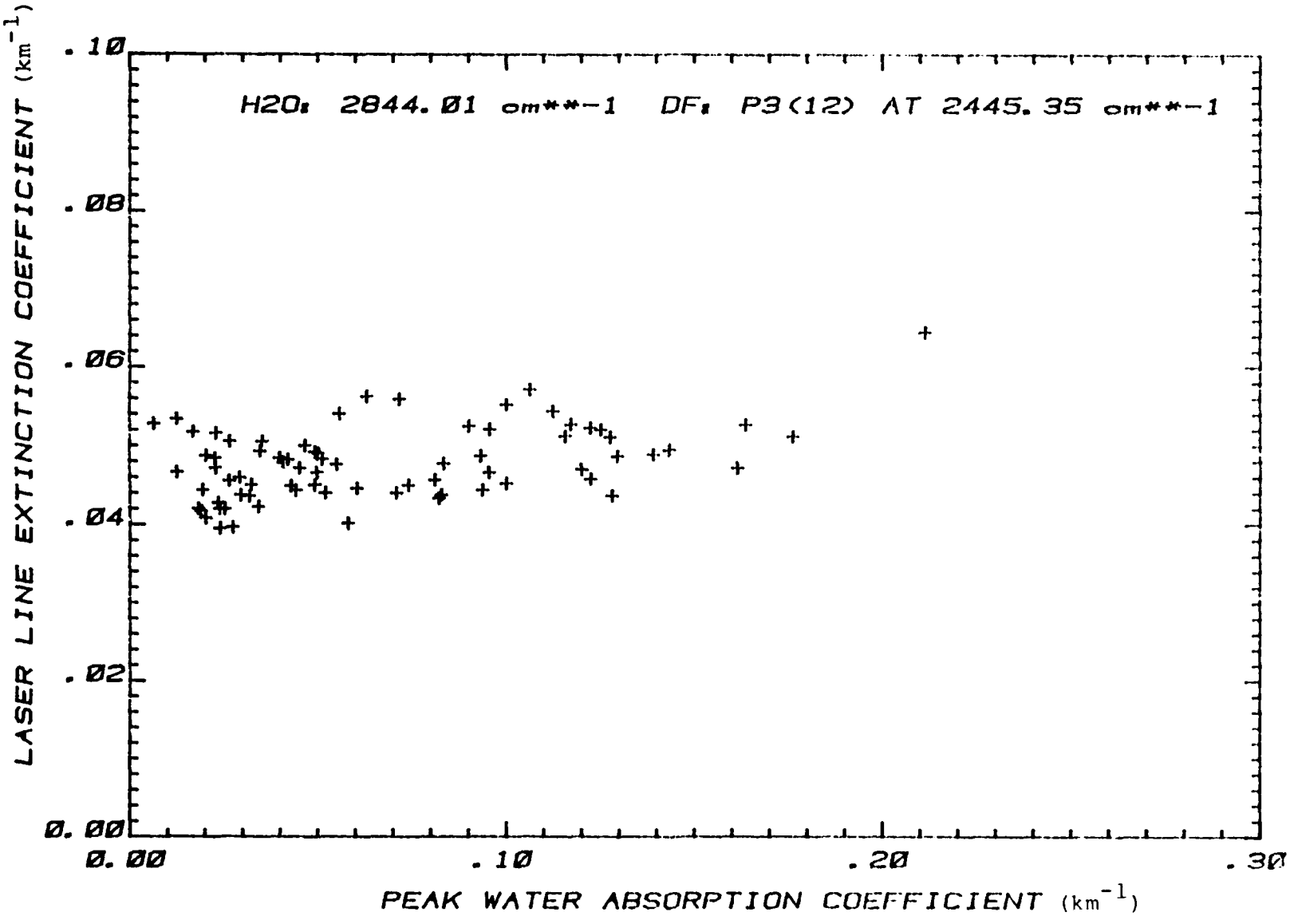

FIGURE 2. EXTINCTION COEFFICIENT AT DF LASER LINE $P_3(12)$ AT 2445.35 cm^{-1} IS PLOTTED AS A FUNCTION OF THE ABSORPTION COEFFICIENT AT THE PEAK OF THE H_2O LINE AT 2844.01 cm^{-1}. EACH POINT REPRESENTS ONE DAY. THE CORRELATION IS WEAK.

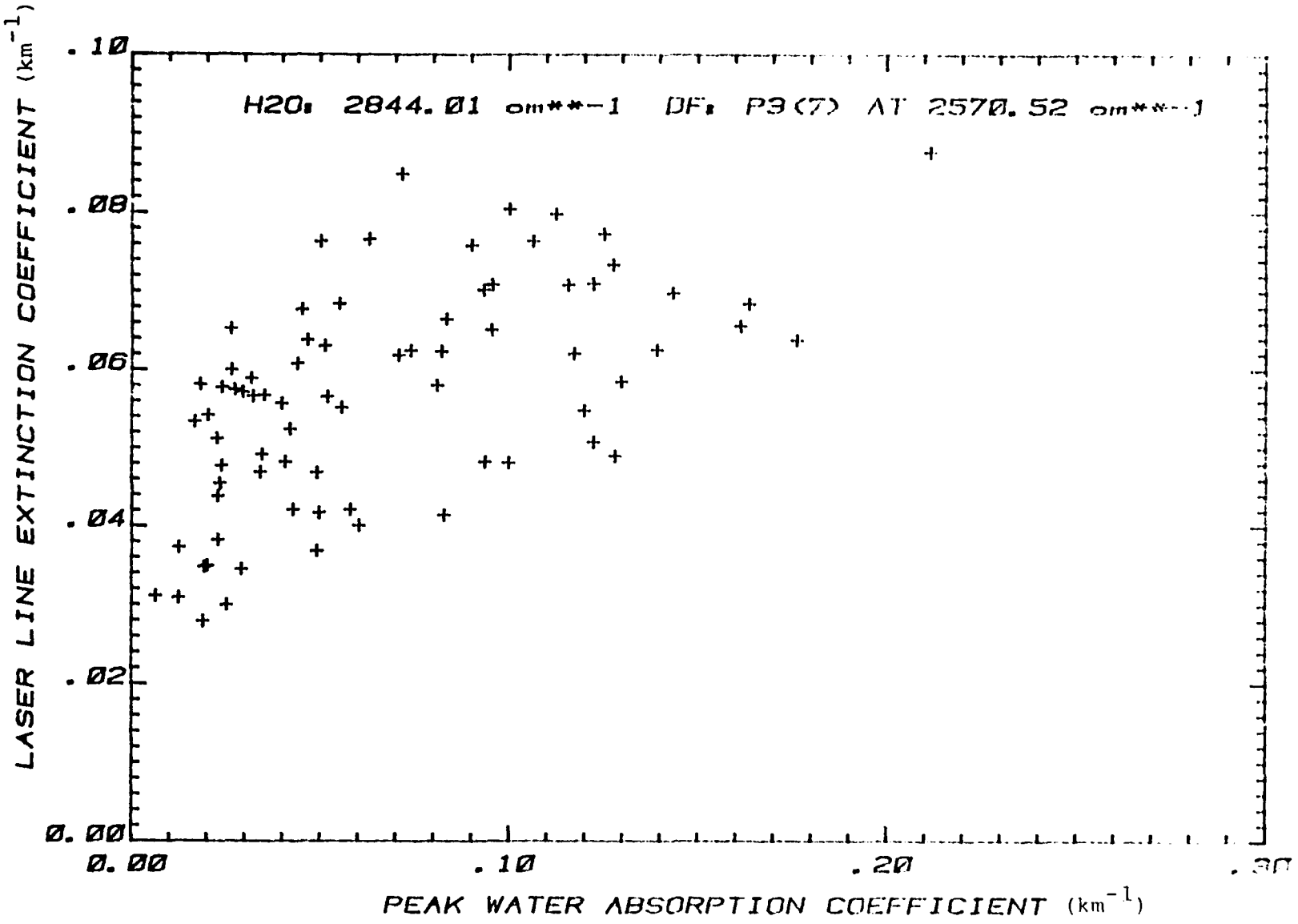

FIGURE 3. EXTINCTION COEFFICIENT AT DF LASER LINE $P_3(7)$ AT 2570.52 cm^{-1} IS PLOTTED AS A FUNCTION OF THE ABSORPTION COEFFICIENT AT THE PEAK OF THE H_2O LINE AT 2844.01 cm^{-1}. EACH POINT REPRESENTS ONE DAY. THE CORRELATION IS WEAK.

at the peak of the H_2O line at 2844.01 cm^{-1}. Figures 4 through 8 are similar plots for 5 CO_2 laser frequencies. Comparing the CO_2 plots with the DF plots is striking. Since the water vapor peak absorption coefficient is related to the total water vapor content along a column in the atmosphere, it appears that the variation in extinctance at the CO_2 frequencies is strongly related to variation in atmospheric water vapor content, while the variation at DF frequencies is due to some other mechanism. It is still not clear, however, whether the CO_2 dependence is due directly to molecular absorption (continuum effects, for instance) or perhaps to water clusters or droplets which themselves depend on water vapor concentration.

3.2 SLANT PATH TRANSMISSION MODEL DEVELOPMENT

Additional analysis of the substantial data base of slant path transmission spectra has proceeded with comparisons to transmission spectra predicted by our current understanding of atmospheric absorption. A recent modeling approach developed by OptiMetrics provides both a high degree of spatial resolution of atmospheric composition with altitude and any desired spectral resolution up to essentially infinite resolution. A high degree of spatial resolution is achieved by using a 25 layer model of the earth's atmosphere with variable layer spacing. Between the earth's surface and 13 km, a minimum spacing of 1 km is used; above 13 km the layer spacing increases, reaching 30 km for the final layer between 70 and 100 km. The basic spectral resolution is infinite and can be convolved with any desired "slit function" to provide comparisons with data acquired by specific hardware (as in this case to a high resolution Michelson interferometer (FTS) used to acquire solar spectra). The spectral resolution of the model

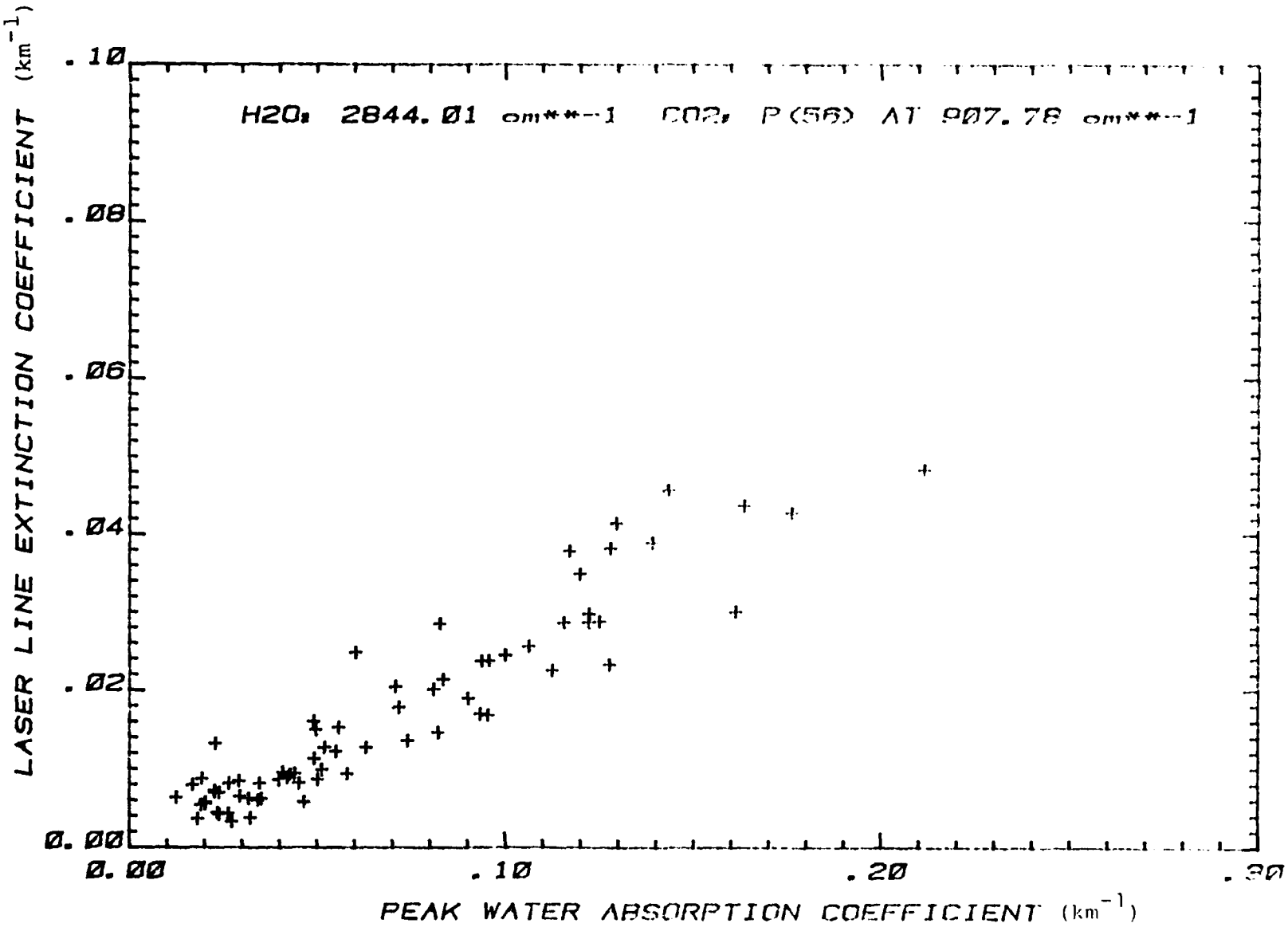

FIGURE 4. EXTINCTION COEFFICIENT AT CO_2 LASER LINE P(56) AT 907.78 cm^{-1} IS PLOTTED AS A FUNCTION OF THE ABSORPTION COEFFICIENT AT THE PEAK OF THE H_2O LINE AT 2844.01 cm^{-1}. EACH POINT REPRESENTS ONE DAY. THE CORRELATION IS RELATIVELY STRONG.

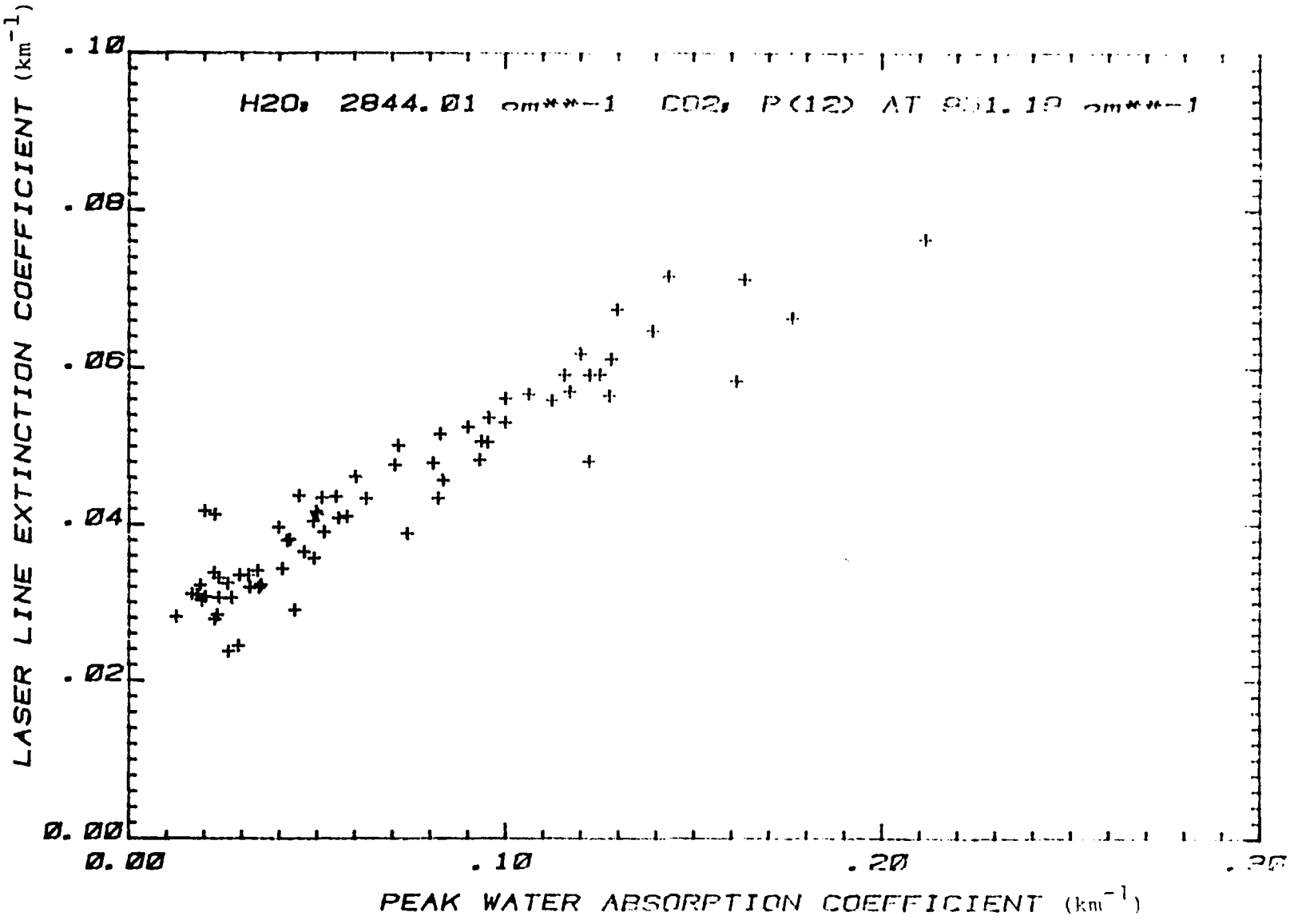

FIGURE 5. EXTINCTION COEFFICIENT AT CO_2 LASER LINE P(20) AT 944.19 cm^{-1} IS PLOTTED AS A FUNCTION OF THE ABSORPTION COEFFICIENT AT THE PEAK OF THE H_2O LINE AT 2844.01 cm^{-1}. EACH POINT REPPESENTS ONE DAY. THE CORRELATION IS RELATIVELY STRONG.

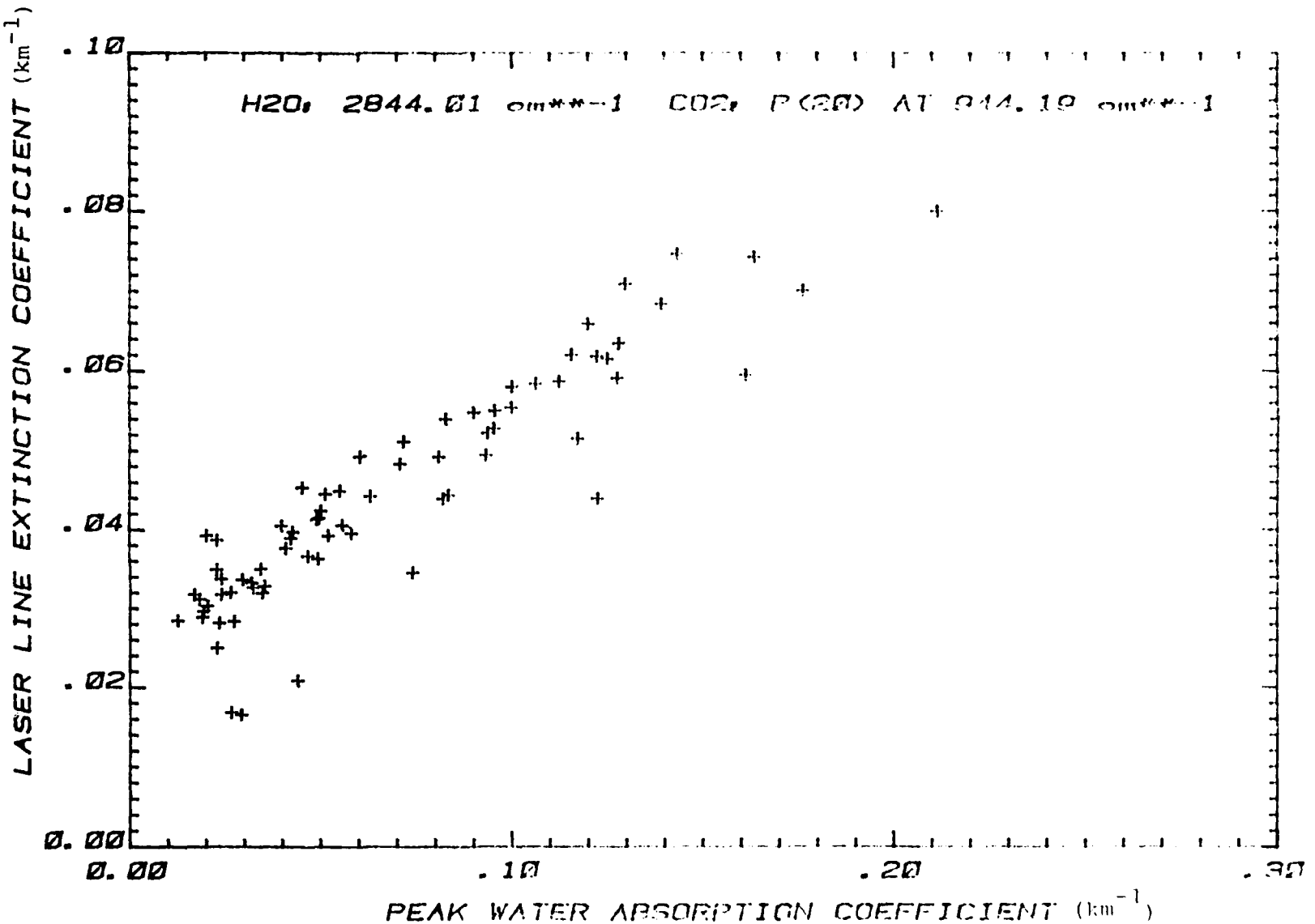

FIGURE 6. EXTINCTION COEFFICIENT AT CO_2 LASER LINE P(12) AT 951.19 cm^{-1} IS PLOTTED AS A FUNCTION OF THE ABSORPTION COEFFICIENT AT THE PEAK OF THE H_2O LINE AT 2844.01 cm^{-1}. EACH POINT REPRESENTS ONE DAY. THE CORRELATION IS RELATIVELY STRONG.

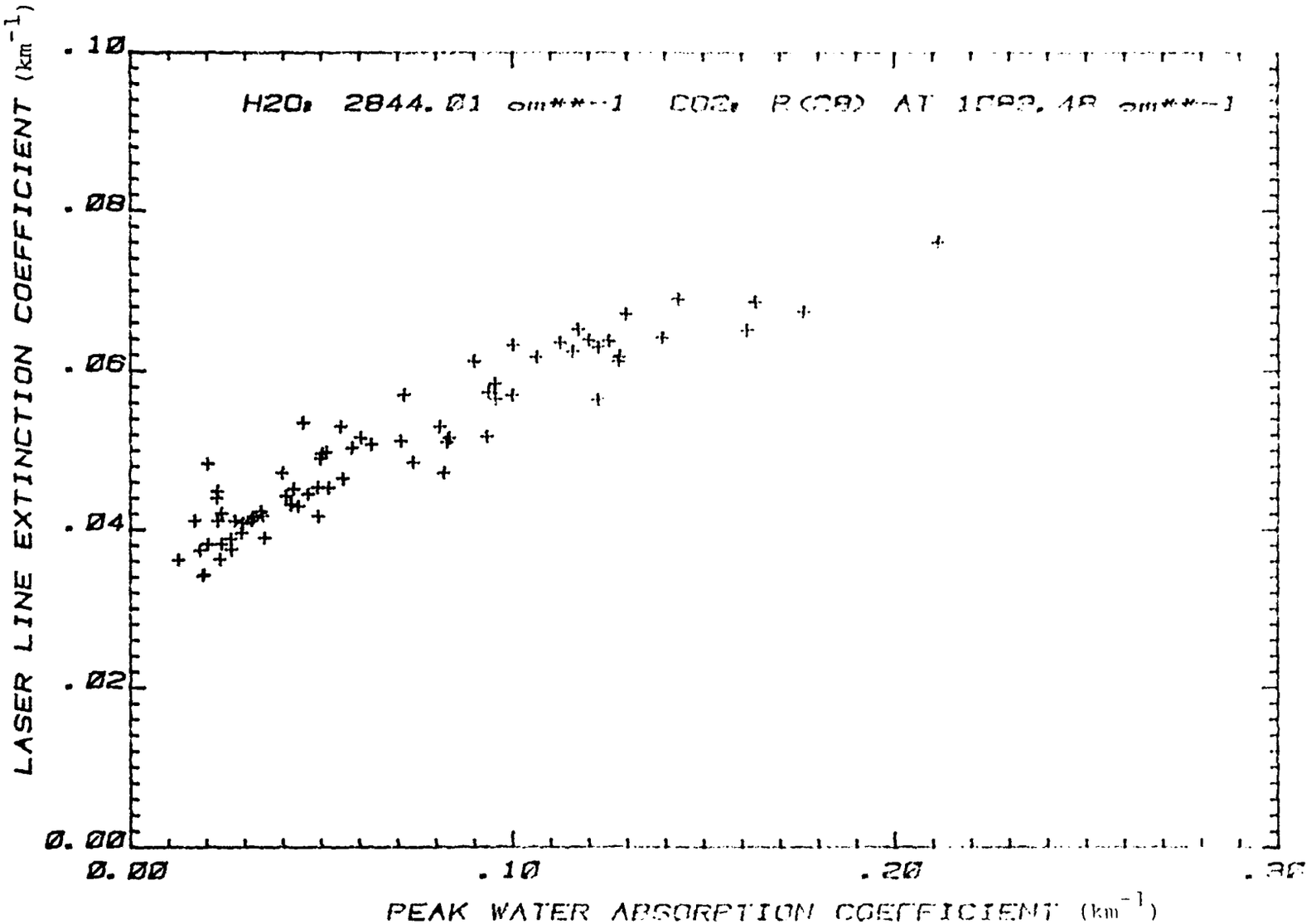

FIGURE 7. EXTINCTION COEFFICIENT AT THE CO_2 LASER LINE R(28) AT 1083.48 cm^{-1} IS PLOTTED AS A FUNCTION OF THE ABSORPTION COEFFICIENT AT THE PEAK OF THE H_2O LINE AT 2844.01 cm^{-1}. EACH POINT REPRESENTS ONE DAY. THE CORRELATION IS RELATIVELY STRONG.

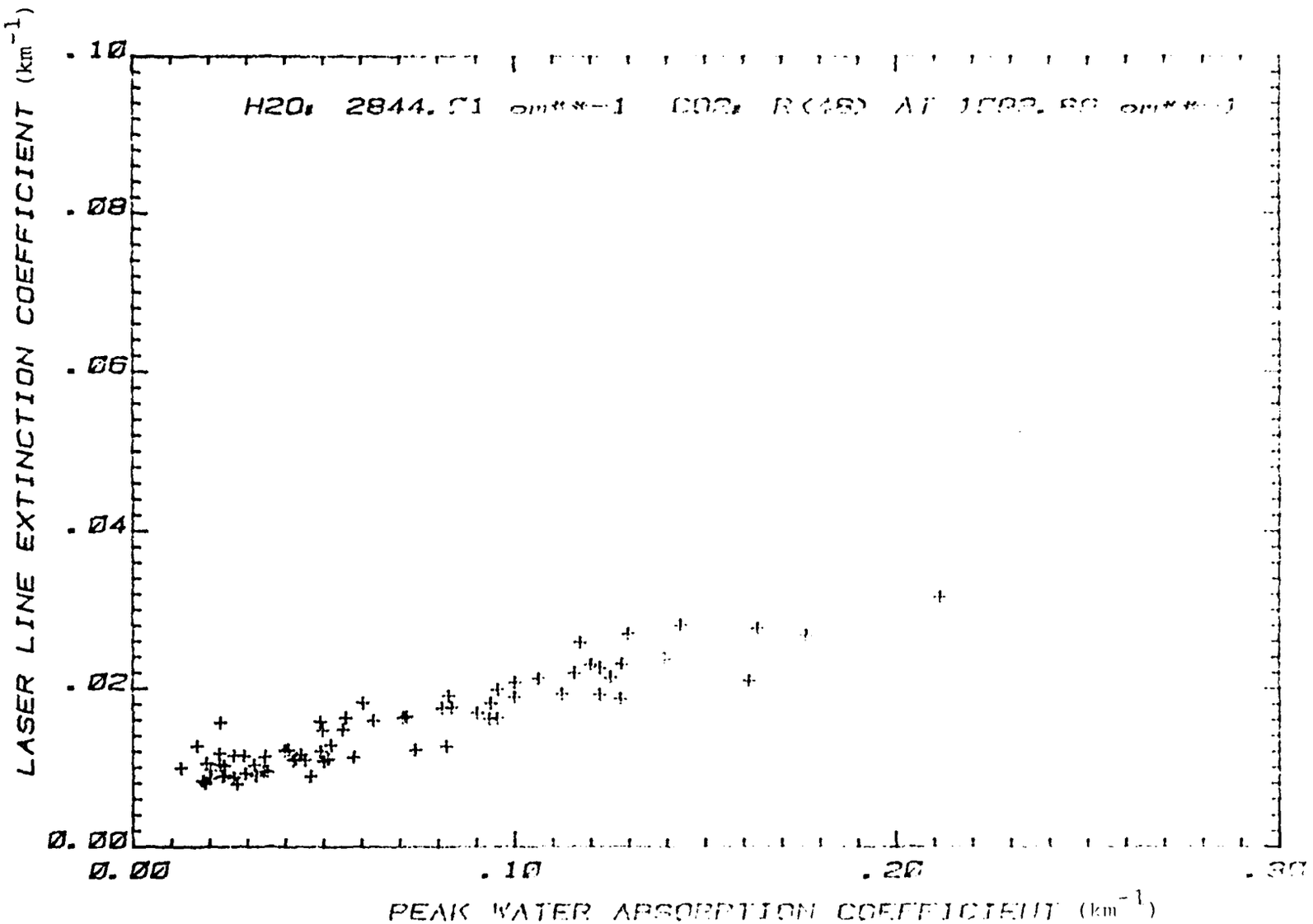

FIGURE 8. EXTINCTION COEFFICIENT AT THE CO_2 LASER LINE R(48) AT 1093.89 cm^{-1} IS PLOTTED AS A FUNCTION OF THE ABSORPTION COEFFICIENT AT THE PEAK OF THE H_2O LINE AT 2844.01 cm^{-1}. EACH POINT REPRESENTS ONE DAY. THE CORRELATION IS RELATIVELY STRONG.

is achieved by use of the AFGL line atlas [4] and by performing line by line molecular absorption calculations. A brief description of the basic calculations used in the model will be given here. The molecular absorption coefficient k(ν) for the absorption of infrared radiation is given by

$$k(\nu) = S f(\nu)$$

where

S is the vibration-rotation transition line strength at temperature T, and

f(ν) is the normalized frequency shape factor.

For near-sea-level atmospheric temperature and pressure the shape factor in frequency space for each molecular transition is closely approximated by the Lorentz function:

$$f(\nu) = \frac{\alpha_L}{\pi(\nu - \nu_o)^2 + \alpha_L^2} \qquad (1)$$

where

ν_o is the transition center frequency, and

α_L is the half width at half maximum amplitude of the absorption line profile.

At lower pressure and temperature (i.e., higher altitudes) as collisions between molecules become more infrequent, the shape factor becomes a convolution of collision and velocity broadening of each absorption transition process. In these cases the shape factor is computed as

$$f(\nu) = \frac{S}{\alpha_D}\frac{\ln 2}{\pi^{3/2}} \int_{-\infty}^{\infty} \frac{e^{-t^2}\,dt}{\left(\frac{\alpha_L}{\alpha_D}\right)^2 \frac{\ln 2}{\pi} + \left[\frac{(\nu - \nu_c)\sqrt{\ln 2}}{\alpha_D} - t\right]^2} \qquad (2)$$

where

α_D is the velocity or Doppler broadened halfwidth at half maximum, and

t is an integration parameter.

This shape factor is often referred to as a Voigt profile and is not normally used in line-by-line calculations because of its complexity. The Voigt profile is used in the OptiMetrics slant path model because of the necessity for high altitude calculations. The line strength S is corrected from the 296 K value given in the AFGL line atlas (S_c) according to the following approximation:

$$S = S_o \frac{P_V^c}{P_V} \frac{P_R^c}{P_R} e^{\frac{E_c(T-T_o)}{TT_o}} \left[\frac{1 - e^{-h\nu_c/kT}}{1 - e^{-h\nu_c/kT_o}}\right] \qquad (3)$$

where P_V is the vibrational partition function which is both temperature and frequency dependent; P_V^o is the value of P_V at the reference temperature T_o (usually 296K). The rotational partition function P_R is only dependent upon temperature; again P_R^o if the value at the reference temperature. The Boltzman factor (given by the two exponential factors in Equation 3) depends upon the lower state energy E_o and the transition frequency ν_o. A more detailed treatment of this subject can be found in References 5 and 6.

Slant path calculations using the OptiMetrics model are based either on atmospheric composition data contained in the computer program for a model atmosphere or on experimental input data when available. The model atmospheres contain vertical density and temperature profiles for each absorber species which are appropriate for different latitudes and seasons and are derived from an average of experimental measurements. Parameter values for these model atmospheres can be found in Reference 5. Important molecular absorption continuum models are included as options for nitrogen and water vapor in the 4 to 5 μm region.

Flexibility of comparison has been built into the slant path transmission model through variable slant path viewing angle and variable viewing platform elevations. The Voigt profile discussed earlier is incorporated through a highly accurate and efficient computational subroutine. Conditions warranting Voigt profile calculations are tested internally for each molecular transition. Super- and sub-Lorentz features are incorporated where specific cases are known to occur as for example, the sub-Lorentz far wings of the 4.3 μm CO_2 bands. The transition line strengths and halfwidths are temperature corrected for accurate calculations between 195 K and 500 K. Calculations outside this interval may be done at reduced accuracy. The temperature dependence of the N_2 collision induced continuum in the 3 - 5 μm region is that found in LOWTRAN-3B (7) and the temperature dependence of the water vapor continuum in the 8 - 14 μm region is that of Roberts (8). Note should be made here, that calculations at wavenumbers below 800 cm^{-1} will be slightly inaccurate until a rigorous expansion of the frequency dependence of the vibrational partition function is incorporated into the model. This can easily be accomplished when necessary at the cost of increased computational time.

3.3 ANALYSIS OF MEASURED FTS SPECTRA

3.3.1 COMPARISONS OF SLANT-PATH TRANSMISSION PREDICTIONS TO MEASURED FTS DATA

Preliminary comparisons of the calibrated slant path transmission spectra to calculated transmission at the same viewing angle were performed using surface parameter data obtained by balloon borne radiosondes. The balloon radiosonde data provided partial pressure of H_2O, total atmospheric pressure and temperature up to 10 km in altitude. Other molecular species concentrations were taken as mid-latitude summer model atmosphere values as were pressure and temperature data when not available from balloon measurements. Figures 9 through 12 show comparisons of model predictions (solid curves) for a 30 cm^{-1} region near 2500 cm^{-1} (4 μm). In the cases considered, the White H_2O continuum model (9) over-predicts absorption while the Burch (10) model under-predicted the measured values. Figure 11 and 12 show examples of comparisons of measured transmission to calculations using the White H_2O continuum model. Figure 13 shows a comparison with the same calculation as shown in Figure 11 except that the Burch continuum model is used. It is interesting to note that the measured transmission is underpredicted by an amount in Figure 11 approximately equal to the overprediction shown in Figure 13. Figure 14 shows the agreement obtained in the 10 μm region using the Roberts, Biberman, and Selby water continuum model (8). All of these calculations were done with a 20 cm^{-1} bound. Considering the complexity of the 25 layer model with independently varying pressure, temperature and molecular density in each layer as well as variable trace gas concentrations and continuum absorption functional dependence, the agreement is remarkable. It appears that the continuum models used here are validated to a reasonable accuracy and

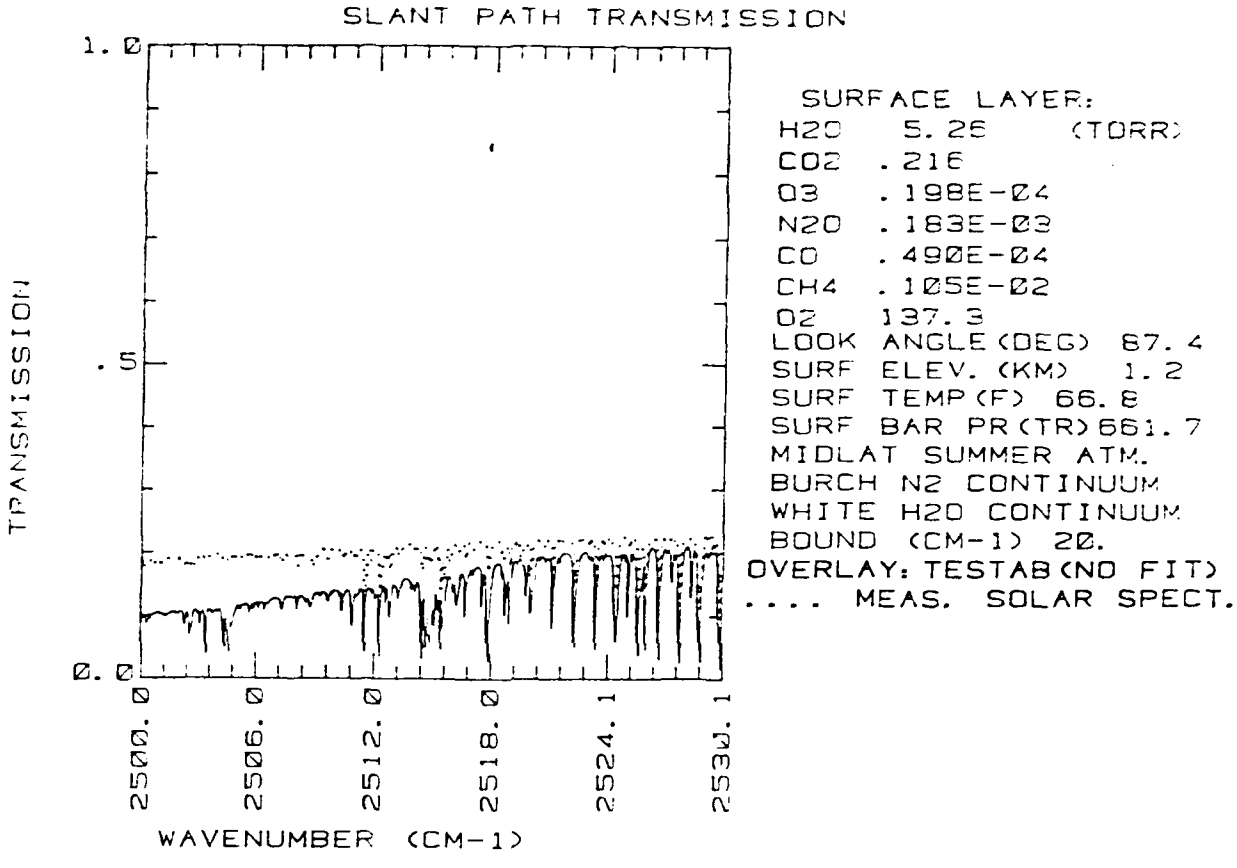

FIGURE 9. SLANT PATH TRANSMISSION SPECTRA AT 4 μm FOR 87.4° FROM ZENITH WITH A 1.21 km SURFACE ELEVATION AND 5.3 TORR PARTIAL PRESSURE H_2O AT SURFACE. THE SOLID CURVE IS THE 25 LAYER MODEL PREDICTION. THE DOTTED CURVE IS THE MEASURED SPECTRA.

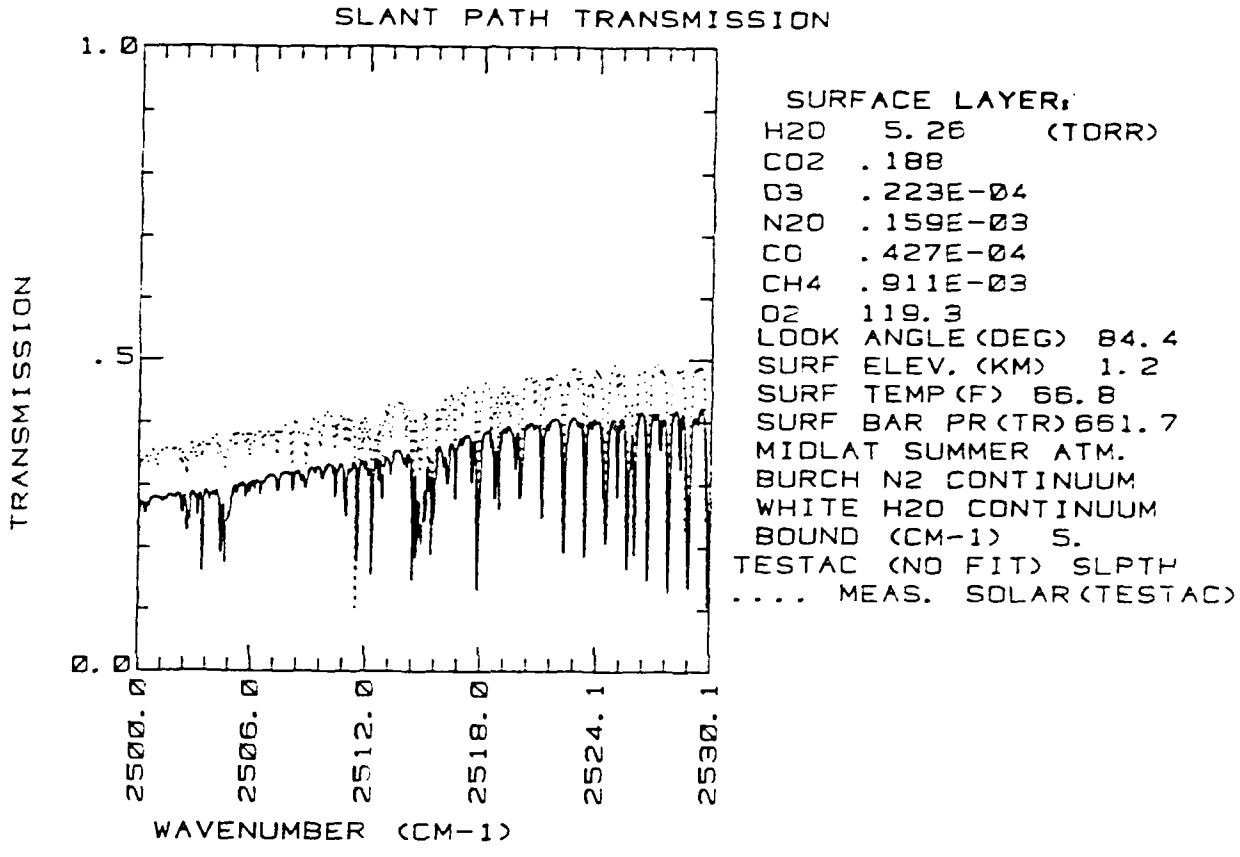

FIGURE 10. SLANT PATH TRANSMISSION SPECTRA AT 4 μm FOR 84.4° FROM ZENITH WITH A 1.23 km SURFACE ELEVATION AND 5.3 TORR H_2O PARTIAL PRESSURE AT SURFACE. THE SOLID CURVE IS THE 25 LAYER MODEL PREDICTION. THE DOTTED CURVE IS THE THE MEASURED SPECTRA.

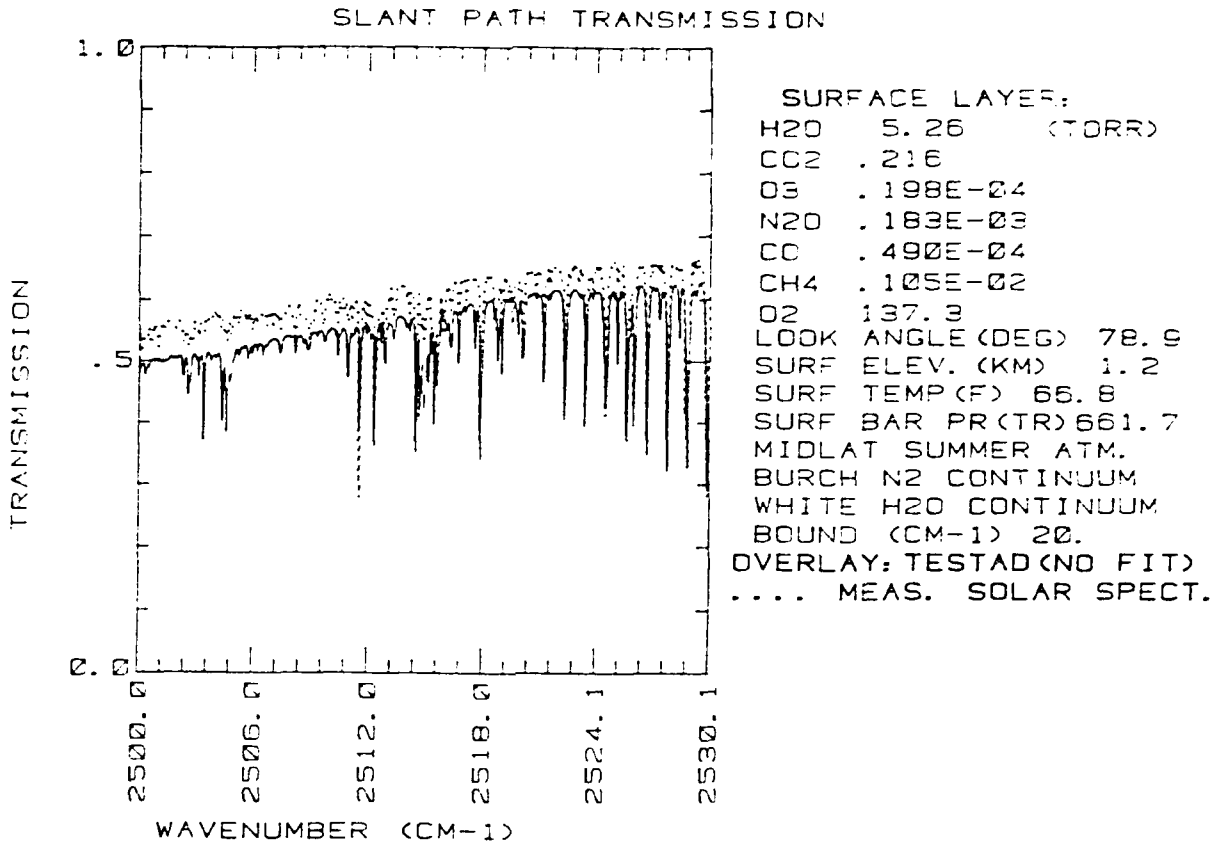

FIGURE 11. SLANT PATH TRANSMISSION SPECTRA AT 4 μm FOR 78.9° FROM ZENITH WITH A 1.21 km SURFACE ELEVATION AND 5.3 TORR PARTIAL PRESSURE OF H_2O AT SURFACE. THE SOLID CURVE IS THE 25 LAYER MODEL PREDICTION. THE DOTTED CURVE IS THE MEASURED SPECTRA.

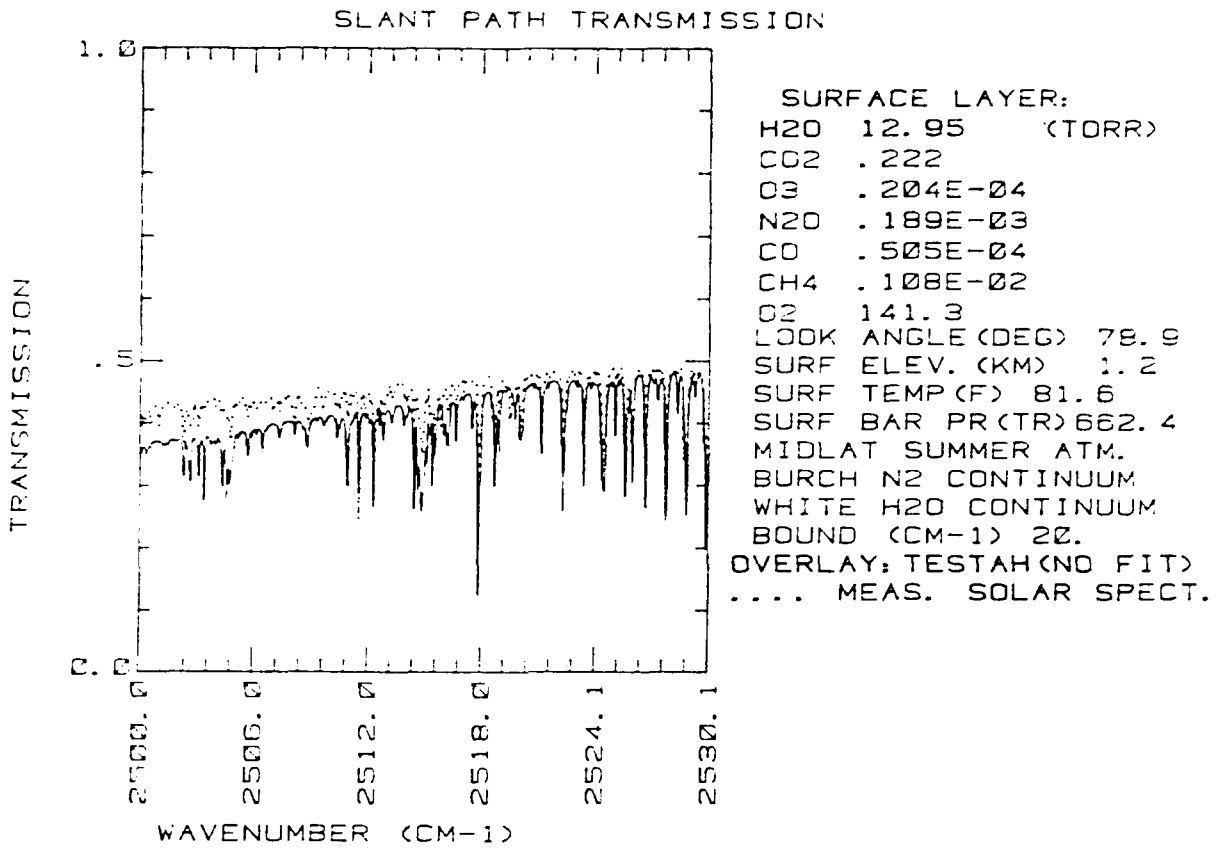

FIGURE 12. SLANT PATH TRANSMISSION SPECTRA AT 4 μm FOR 78.9° FROM ZENITH WITH A 1.21 km SURFACE ELEVATION AND 12.9 TORR PARTIAL PRESSURE OF H_2O AT SURFACE. THE SOLID CURVE IS THE 25 LAYER MODEL PREDICTION. THE DOTTED CURVE IS THE MEASURED SPECTRA.

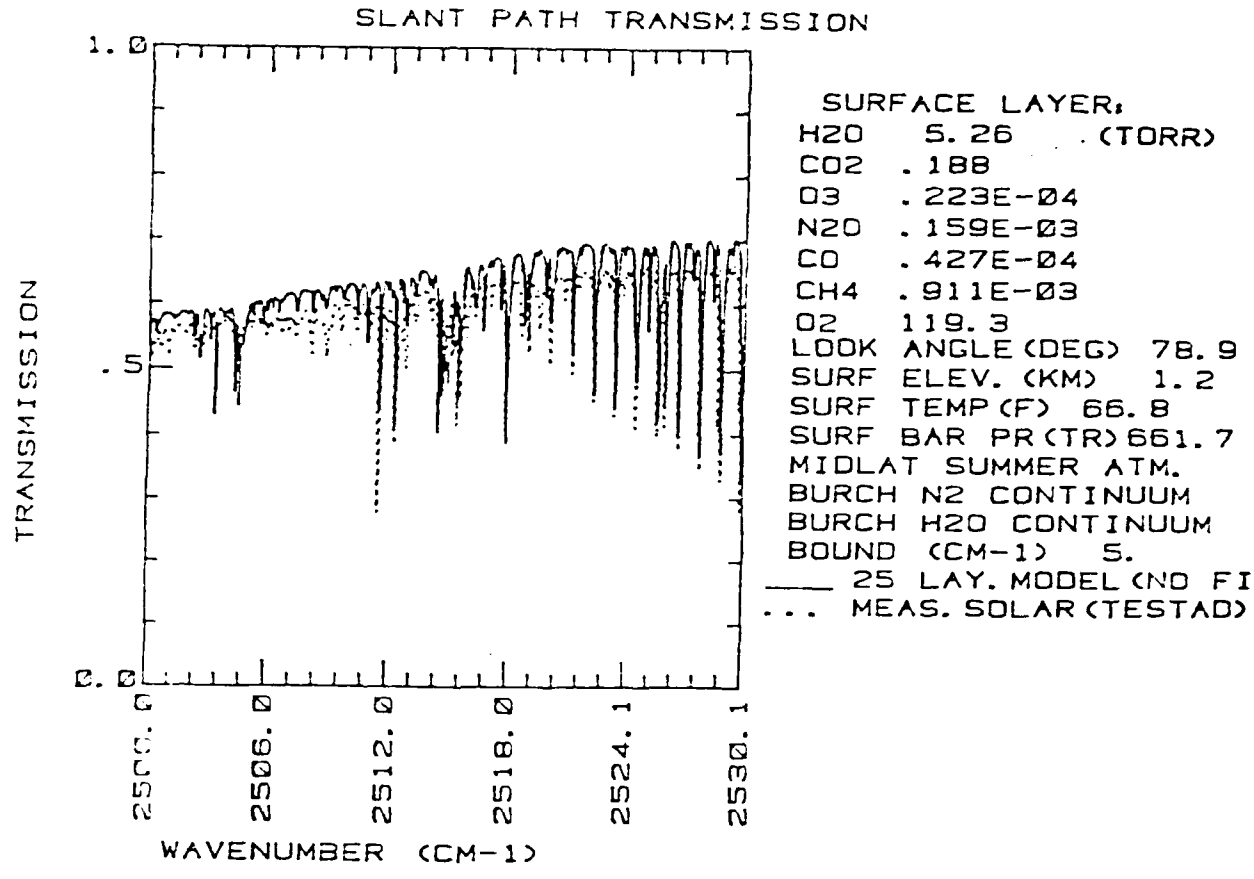

FIGURE 13. SLANT PATH TRANSMISSION SPECTRA AT 4 μm WITH SAME CONDITIONS AS FIGURE 11 EXCEPT A BURCH WATER VAPOR CONTINUUM IS USED INSTEAD OF THE WHITE WATER VAPOR CONTINUUM.

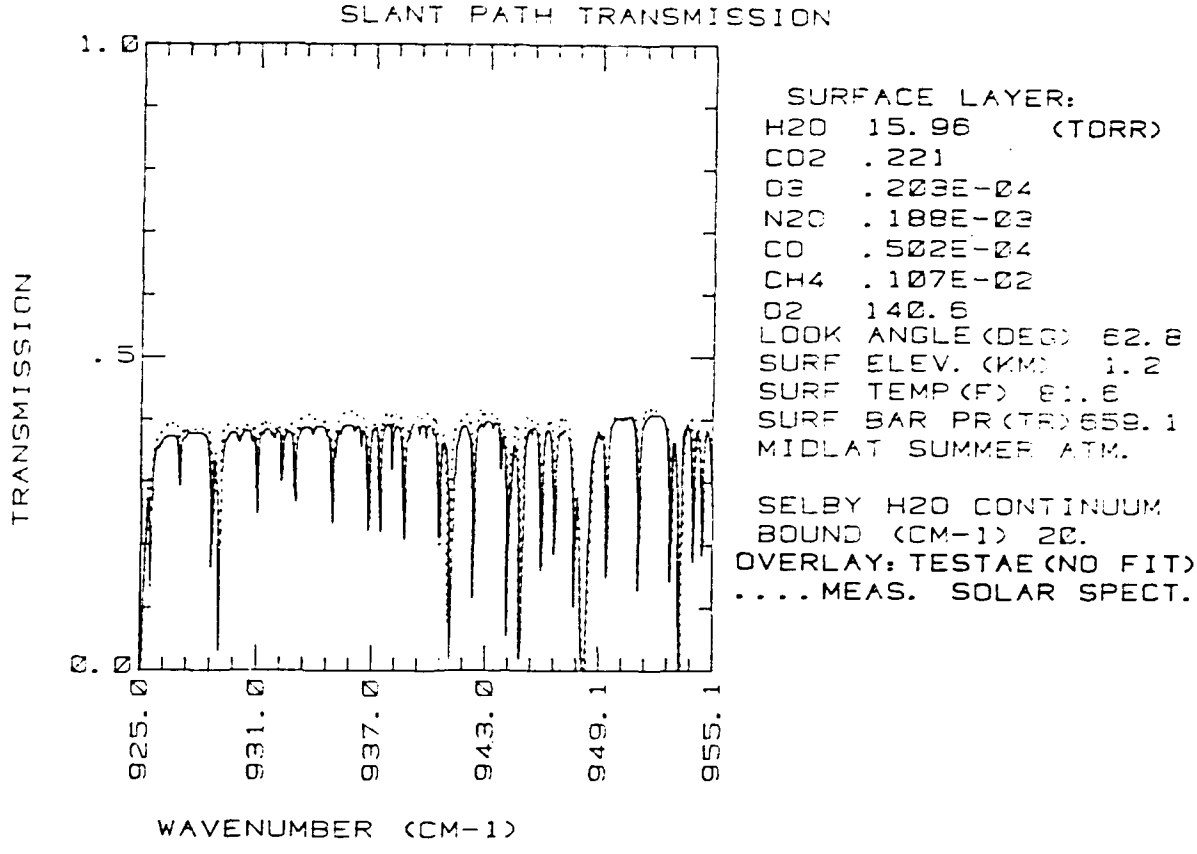

FIGURE 14. SLANT PATH TRANSMISSION SPECTRA AT 10.6 μm FOR 62.8° FROM ZENITH WITH A 1.21 km SURFACE ELEVATION AND 16 TORR PARTIAL PRESSURE OF H_2O AT SURFACE. THE SOLID CURVE IS THE 25 LAYER MODEL PREDICTION. THE DOTTED CURVE IS THE MEASURED SPECTRA.

only require minor adjustments to the temperature and spectral dependence of the continuum absorption coefficient. Additional spectra should be acquired and compared to the code to assess the temperature dependence and the variations in spectral dependence that are apparent in Figure 9. Due to the strong temperature lapse in the lower 10 km of the atmosphere where significant amounts of H_2O occur, a sensitive test of H_2O continuum absorption temperature dependence is now available. This test is free from problems associated with instrument calibrations, contaminants, detector instabilities and the poisoning or quenching effects of limited laboratory cell dimensions on long range intermolecular forces which may exist and possibly contribute to continuum absorption. The comparisons of the measured FTS spectra to the slant path calculations for the 2500 cm^{-1} to 2530 cm^{-1} region shown in Figures 9 - 13 also demonstrate that the observed strengths of certain H_2O transitions near 2503 cm^{-1} and 2511 cm^{-1} disagree with the values listed in the AFGL line atlas (4).

One of the most important results of this work is the capability to accurately predict slant path transmission at any wavelength contained in the AFGL line atlas, and for any elevation angle and initial platform altitude. This means that the complexity of systems' performance analyses along atmospheric slant paths can be reduced to a balloon measurement of the vertical profile of H_2O and a computer calculation. Of course other spectral regions need to be compared to the AFGL atlas and validated in a similar manner before confidence in the atlas values in these regions can be established. The slant path transmission calculation for this 25 layer model can be completed in 15 minutes or less depending upon the computer used.

3.3.2 EXTRACTION OF VERTICAL DENSITY PROFILES OF ABSORBING SPECIES FROM MEASURED FTS DATA

Another important utilization of the calibrated slant-path transmission spectra although much more complex than the comparisons discussed thus far is the extraction of vertical density profiles of any IR absorbing species contained in the line atlas from the FTS data. Using refinements of the comparison technique previously described it becomes possible to substitute slant path solar FTS measurements for the balloon borne radiosonde data. The balloon monitors only those parameters for which it is specifically instrumented -- typically H_2O partial pressure, total pressure and temperature. Significant problems can arise when the large surface area of the balloon contaminates the local atmosphere near the sensor upon ascension as the balloon carries with it H_2O vapor from the denser lower layers of the atmosphere.

The profile extraction code uses an algorithm which computes three candidate atmospheric transmission spectra for differing profiles of the species being studied and tests the root mean square deviation of these test spectra from the measured solar spectra being fit. A best profile is selected and the procedure is repeated using the new best atmospheric concentration profile as a mean and smaller deviations than in the previous iteration. Improved convergence to the best rms fit was achieved by scaling the first 10 km path segment without a vertical gradient at first and then fitting a skew factor to this 10 km segment before stepping through each layer individually, starting at the surface, to look for small irregularities. This approach was found to be satisfactory for all cases except possible large temperature inversions, in which case an average result was obtained that did not reproduce the inversion.

Figures 15a through 19a, show the results of the best fit computed spectrum compared to the measured solar spectra and Figures 15b through 19b show the corresponding vertical H_2O concentration profiles compared to balloon data taken close in time. The comparisons show generally good agreement near the ground with the balloon reading showing relatively higher water vapor at middle elevations and the two profiles in much better agreement above 7 km. It should be pointed out again that a possible explanation for the balloon reading being high on ascension even when calibrated to an absolute reading at the surface is that water vapor absorbed on the large surface area of the balloon is carried from regions of higher to lower density as the balloon climbs. If we accept the balloon data as accurate, then the model values for the H_2O continuum should be adjusted to produce better agreement.

The uncertainty in the extracted vertical density profiles was checked by choosing a-priori an arbitrary water density profile and inputting this profile into the 25 layer transmission model to generate a synthetic slant-path transmission. This noise-free spectrum was then used by the 25 layer vertical density profile fitting routine to extract a profile. The results of this test case are shown in Figure 20a. Here the solid curve is the transmission spectrum corresponding to the assumed H_2O density profile and the dotted curve is the least squares fit to this test spectrum obtained with 25 layer model using the vertical density profile of H_2O as the parameter being fitted. Figure 20b shows the H_2O density profile resulting from the fit to the synthetic transmission spectrum with no other inputs. As can be seen, maximum deviations in H_2O density with altitude are less than 10% with most points much closer.

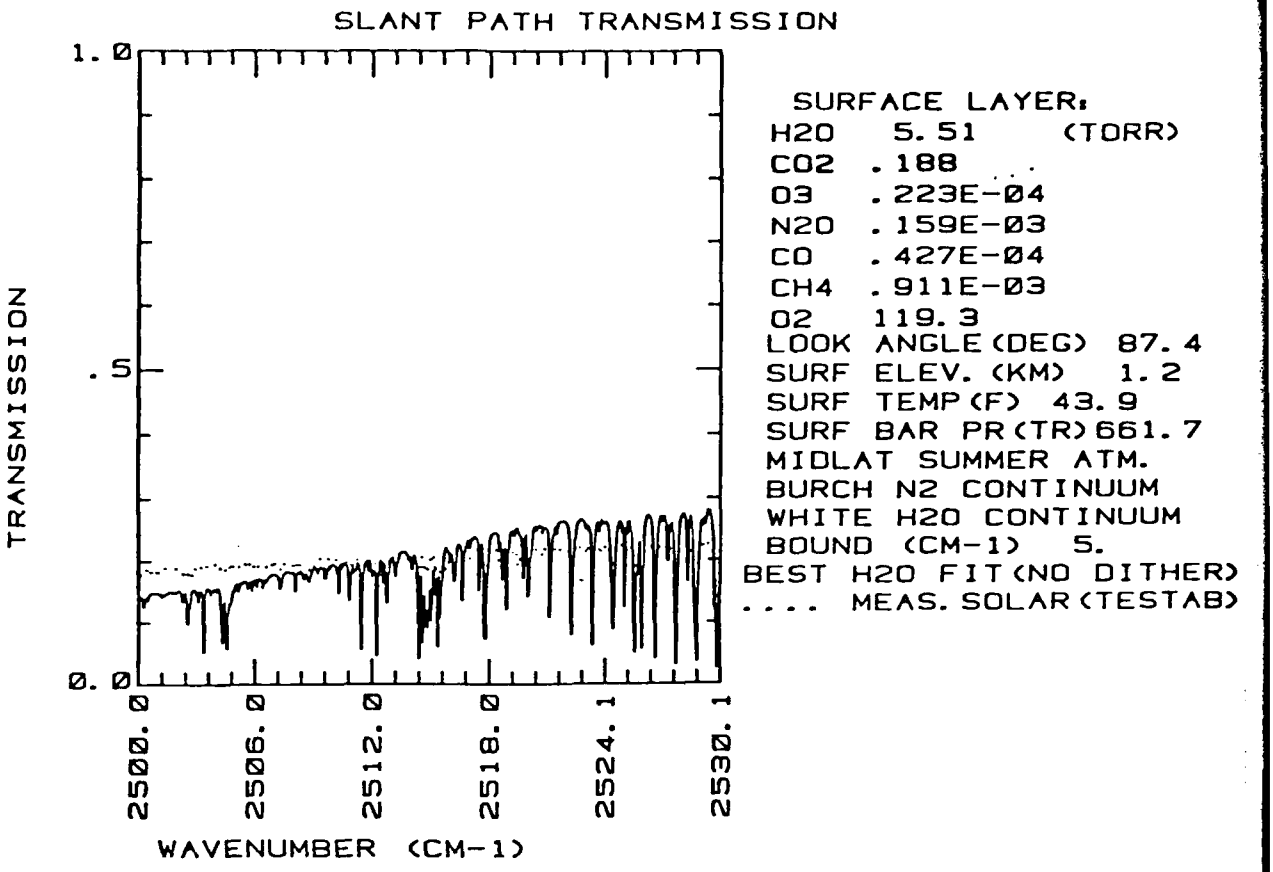

FIGURE 15a. THE SOLID CURVE IS A LEAST SQUARES FIT OF THE 25 LAYER MODEL, WITH H_2O AS THE SEARCH PARAMETER, TO THE MEASURED SLANT PATH TRANSMISSION SPECTRUM SHOWN AS THE DOTTED CURVE FOR THE CONDITIONS GIVEN ON THE FIGURE.

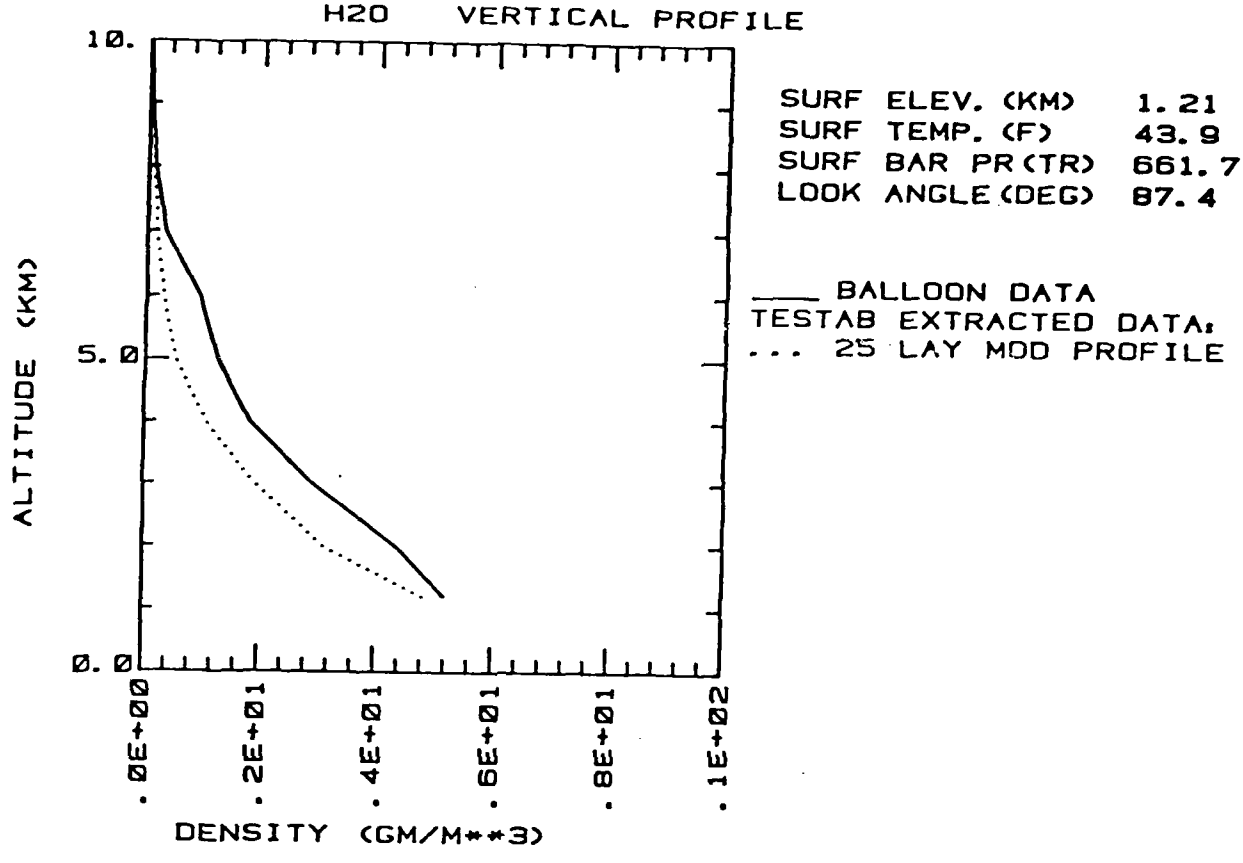

FIGURE 15b. THE H_2O VERTICAL DENSITY PROFILE RESULTING FROM THE BEST FIT SPECTRUM GIVEN IN FIGURE 15a IS SHOWN AS THE DOTTED CURVE. THE SOLID CURVE IS A BALLOON BORNE RADIOSONDE MEASUREMENT TAKEN THE SAME DAY IN THE MORNING.

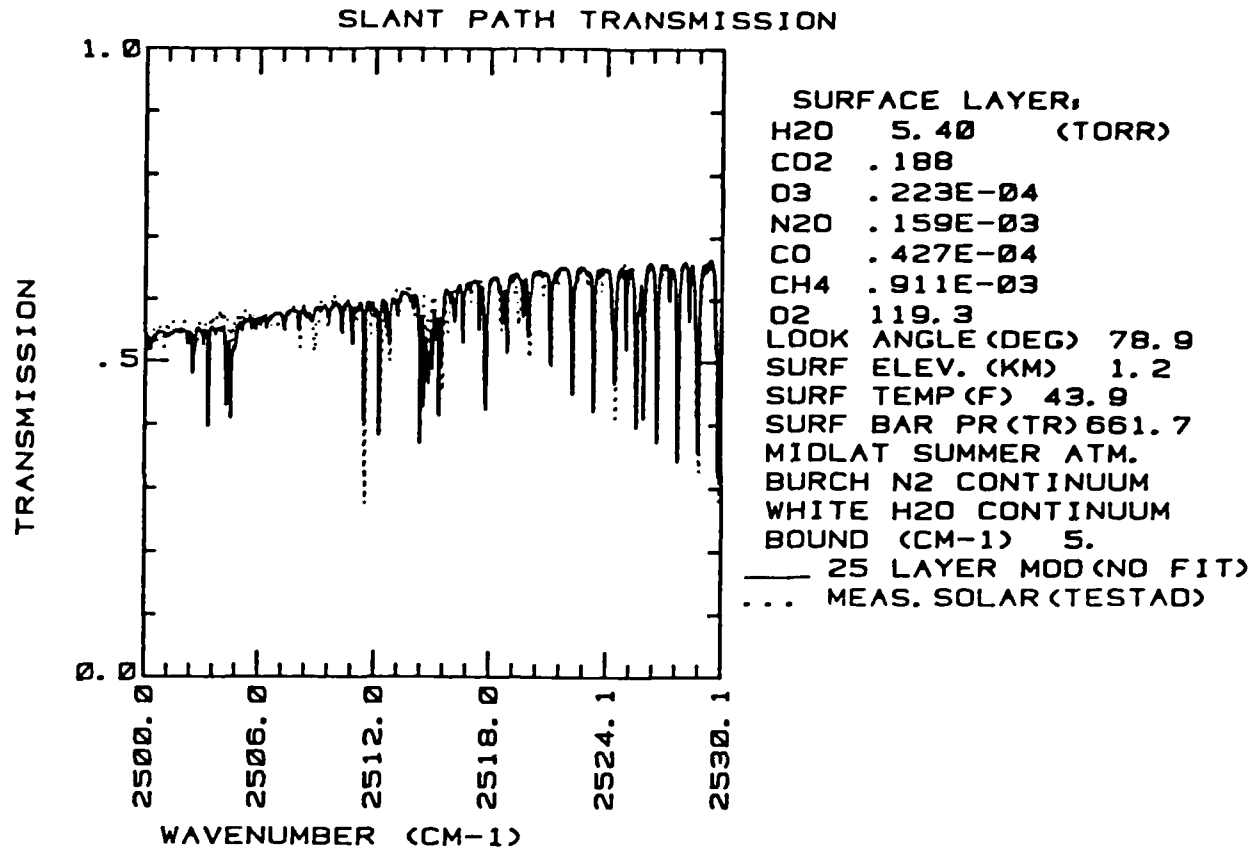

FIGURE 16a. THE SOLID CURVE IS A LEAST SQUARES FIT OF THE 25 LAYER MODEL, WITH H_2O AS THE SEARCH PARAMETER, TO THE MEASURED SLANT PATH TRANSMISSION SPECTRUM SHOWN AS THE DOTTED CURVE FOR THE CONDITIONS ON THE FIGURE.

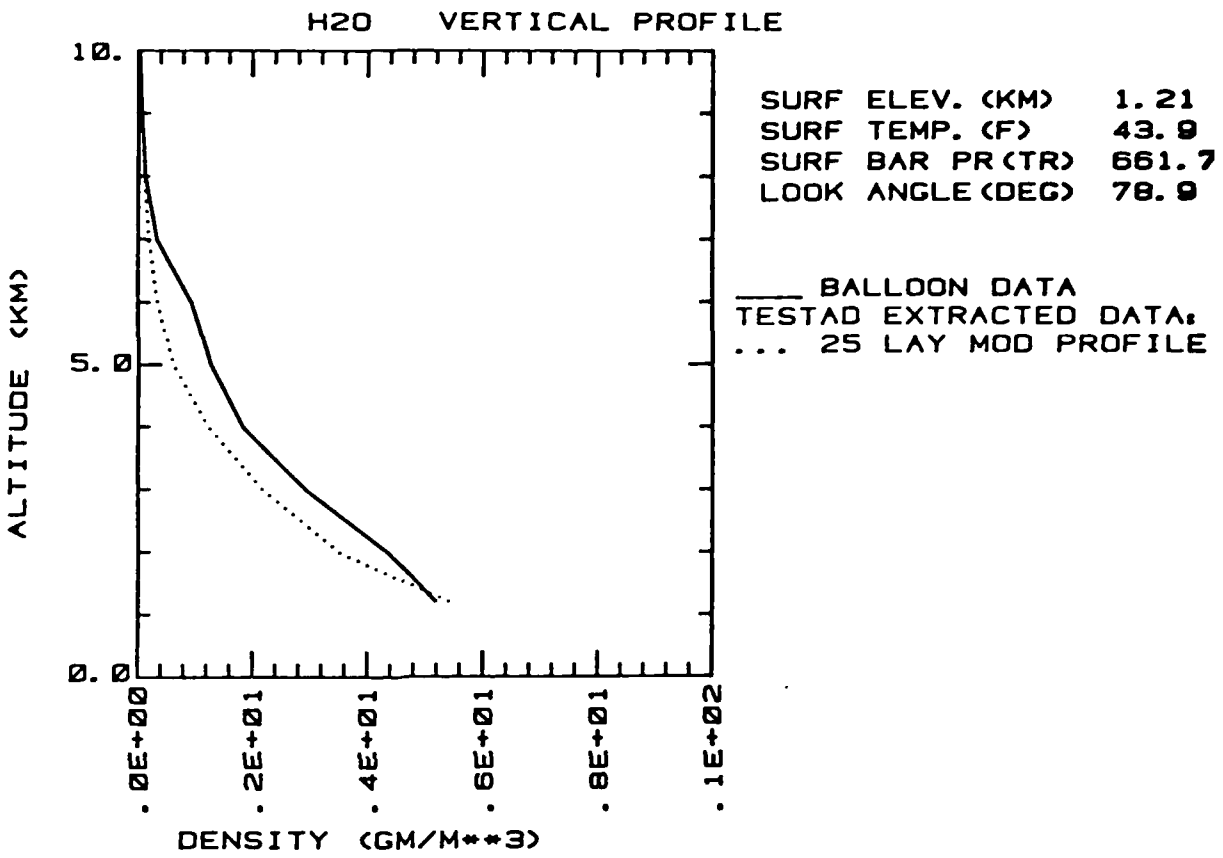

FIGURE 16b. THE H_2O VERTICAL DENSITY PROFILE RESULTING FROM THE BEST FIT SPECTRUM GIVEN IN FIGURE 16a IS SHOWN AS THE DOTTED CURVE. THE SOLID CURVE IS A BALLOON BORNE RADIOSONDE MEASUREMENT TAKEN THE SAME DAY IN THE MORNING.

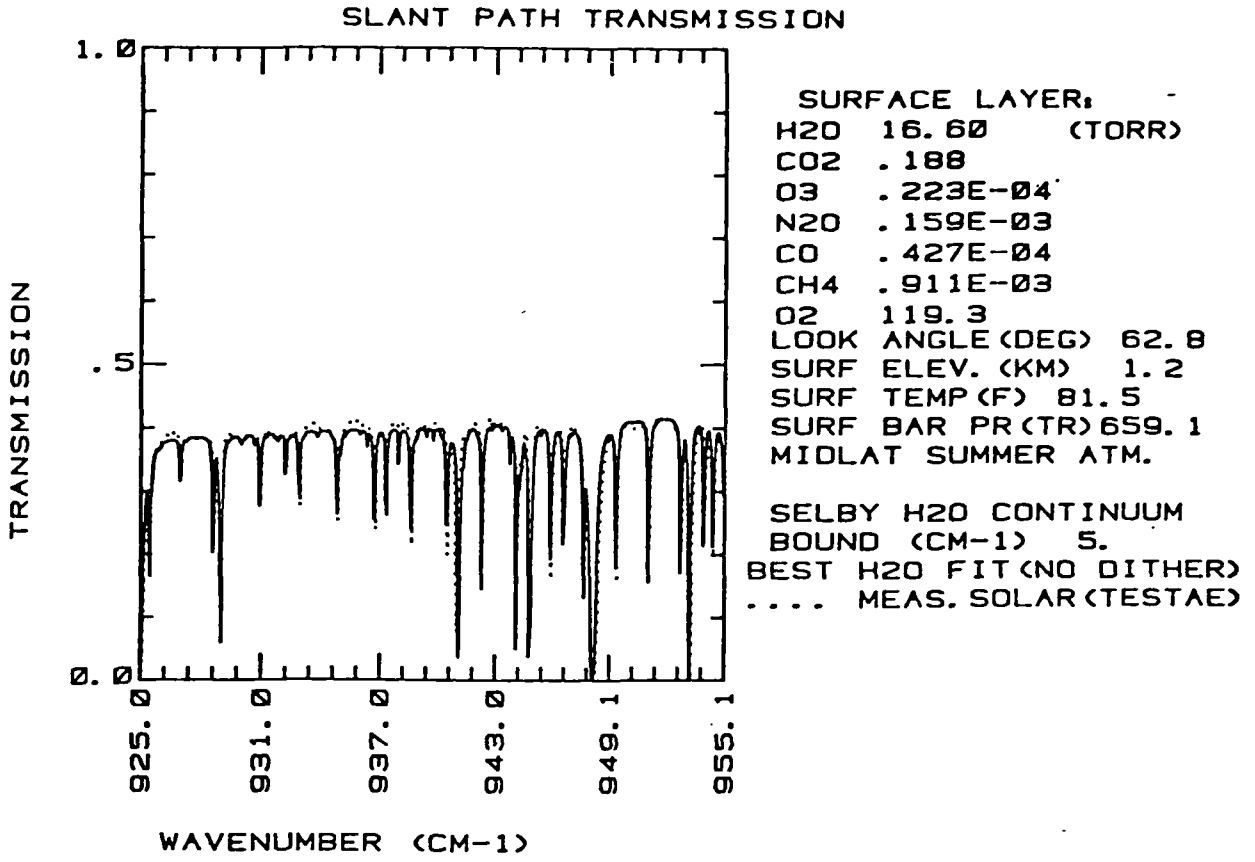

FIGURE 17a. THE SOLID CURVE IS A LEAST SQUARES FIT OF THE 25 LAYER MODEL, WITH H_2O AS THE SEARCH PARAMETER, TO THE MEASURED SLANT PATH TRANSMISSION SPECTRUM CONDITIONS GIVEN ON THE FIGURE.

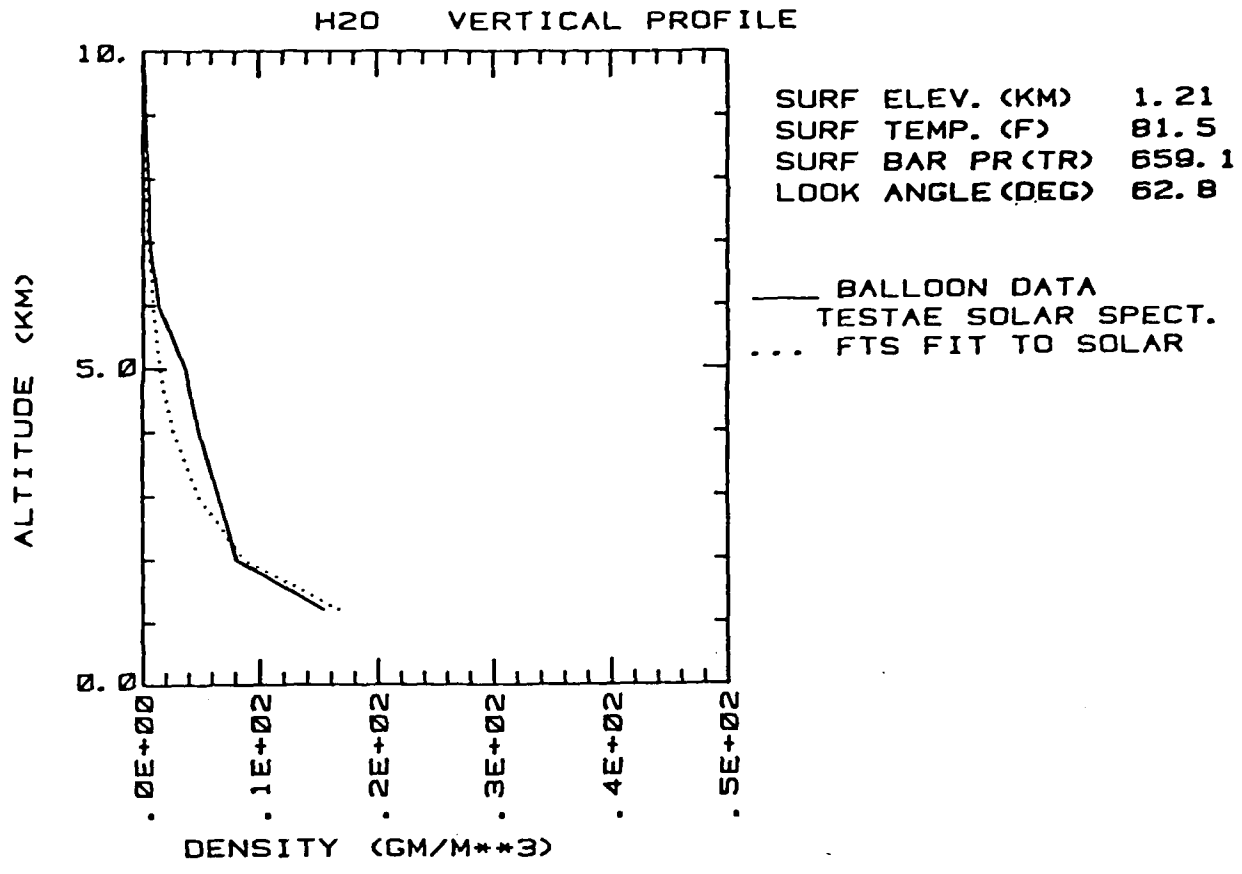

FIGURE 17b. THE H_2O VERTICAL DENSITY PROFILE RESULTING FROM THE BEST FIT SPECTRUM GIVEN IN FIGURE 17a IS SHOWN AS THE DOTTED CURVE. THE SOLID CURVE IS A BALLOON BORNE RADIOSONDE MEASUREMENT TAKEN THE SAME DAY IN THE MORNING.

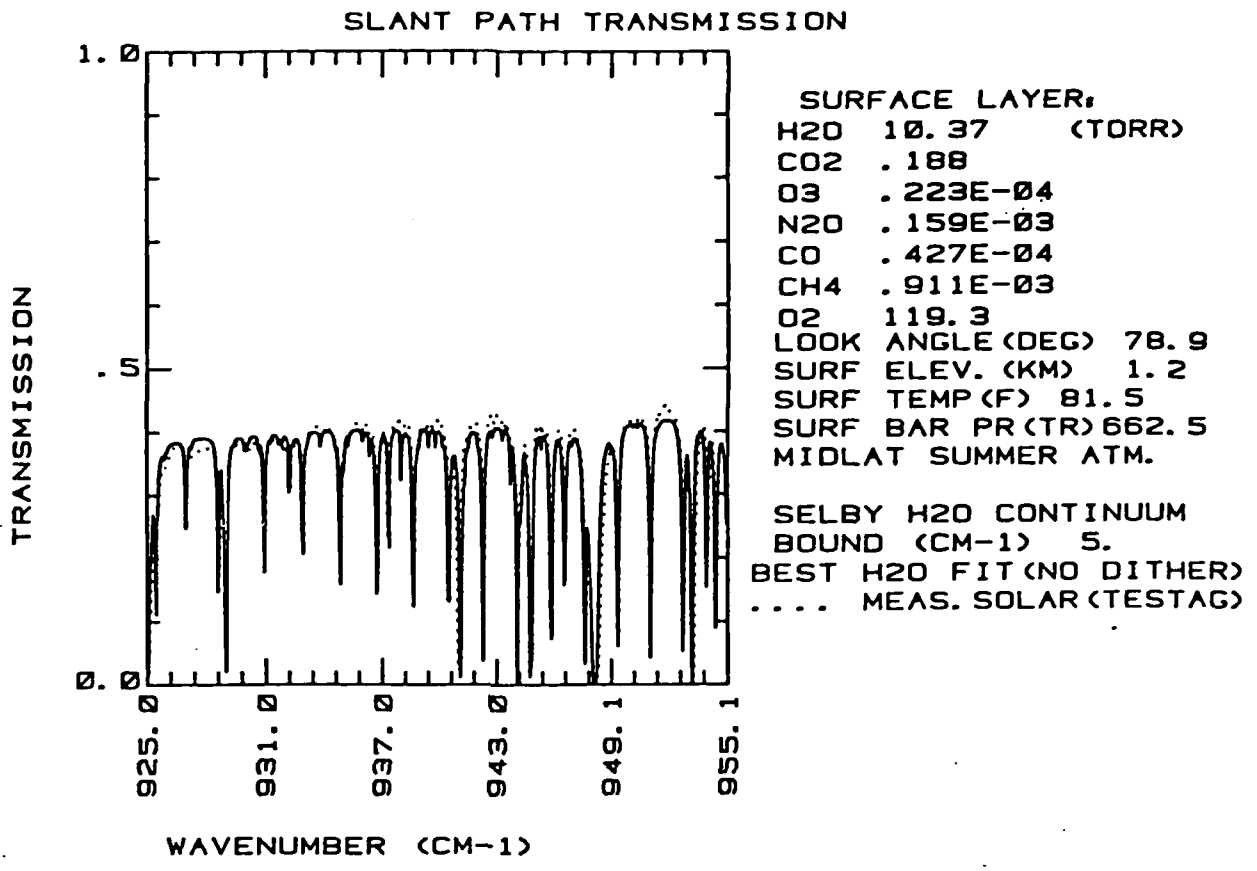

FIGURE 18a. THE SOLID CURVE IS A LEAST SQUARES FIT OF THE 25 LAYER MODEL, WITH H_2O AS THE SEARCH PARAMETER, TO THE MEASURED SLANT PATH TRANSMISSION SPECTRUM SHOWN AS THE DOTTED CURVE FOR THE CONDITIONS GIVEN ON THE FIGURE.

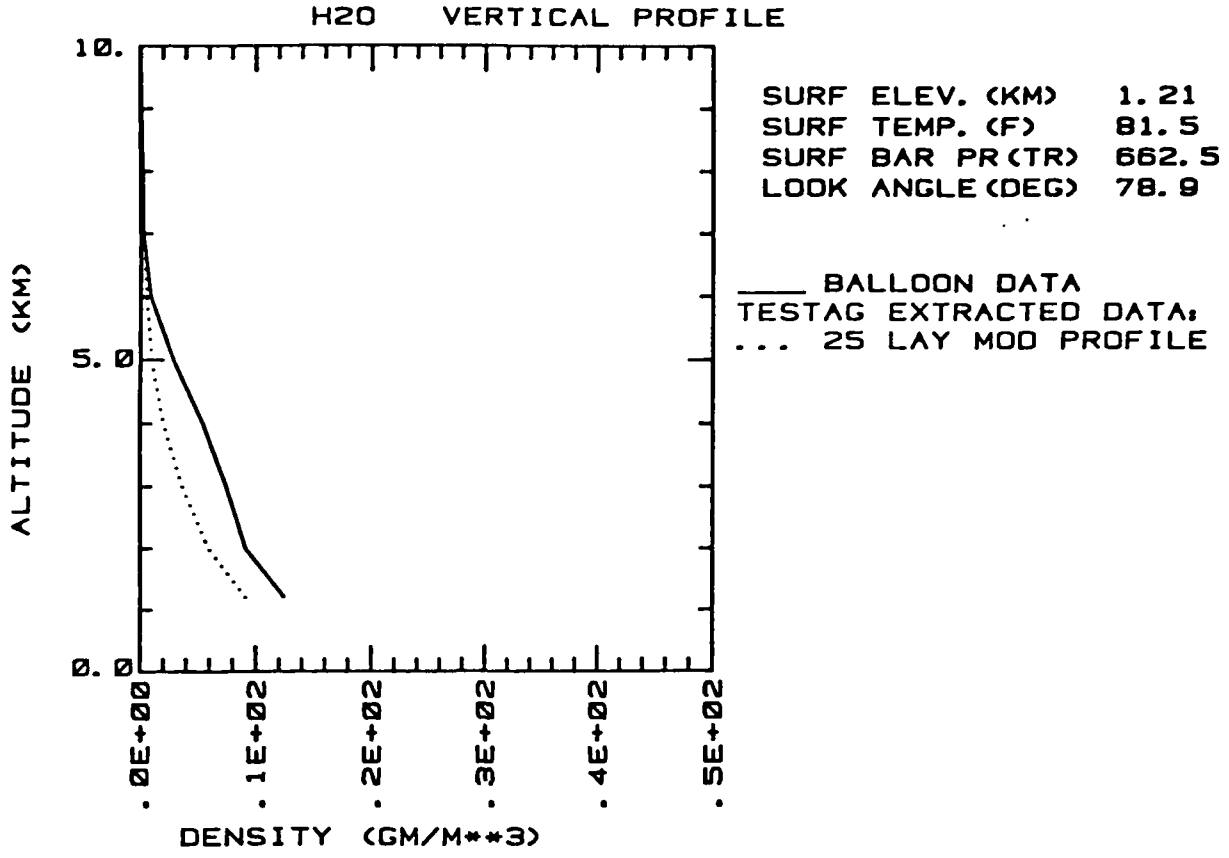

FIGURE 18b. THE H_2O VERTICAL DENSITY PROFILE RESULTING FROM THE BEST FIT SPECTRUM GIVEN IN FIGURE 18a IS SHOWN AS THE DOTTED CURVE. THE SOLID CURVE IS A BALLOON BORNE RADIOSONDE MEASUREMENT TAKEN THE SAME DAY IN THE MORNING.

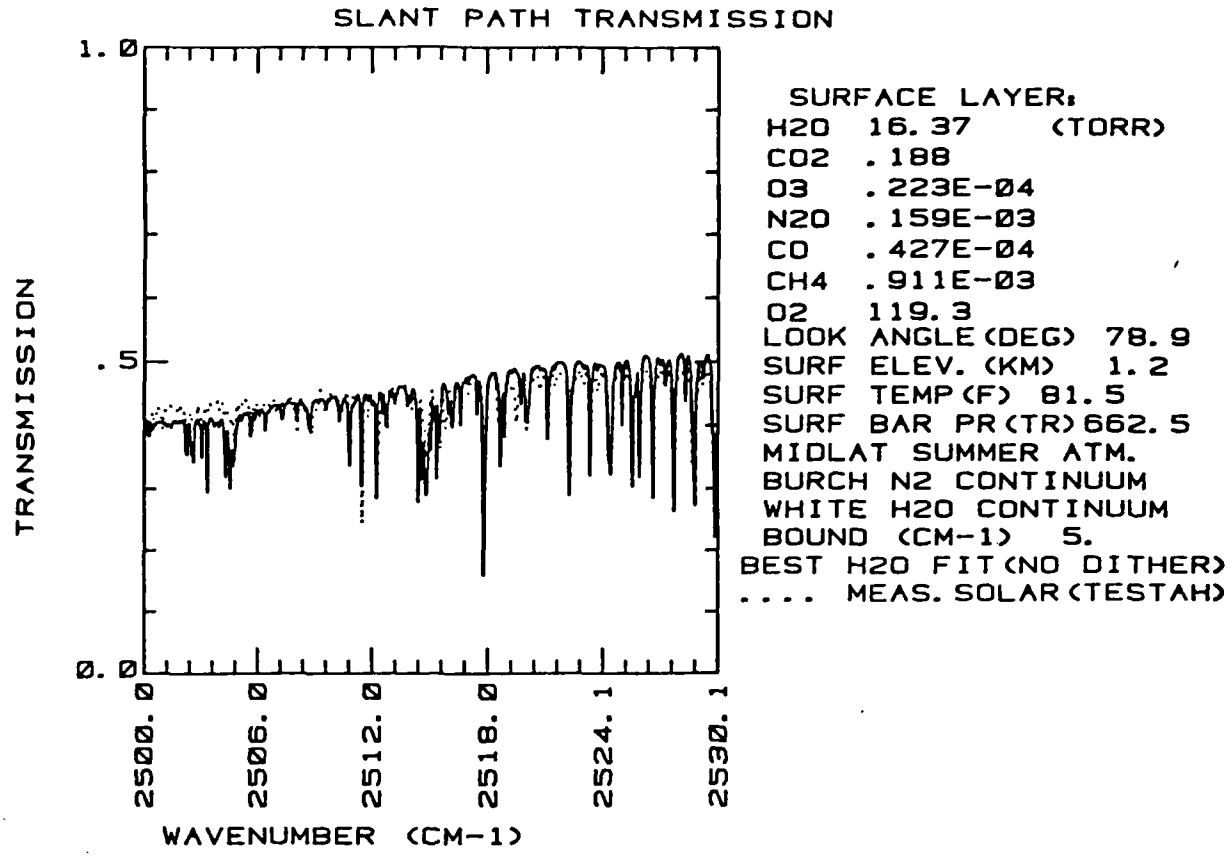

FIGURE 19a. THE SOLID CURVE IS A LEAST SQUARES FIT OF THE 25 LAYER MODEL, WITH H_2O AS THE SEARCH PARAMETER, TO THE MEASURED SLANT PATH TRANSMISSION SPECTRUM SHOWN AS THE DOTTED CURVE FOR THE CONDITIONS GIVEN ON THE FIGURE.

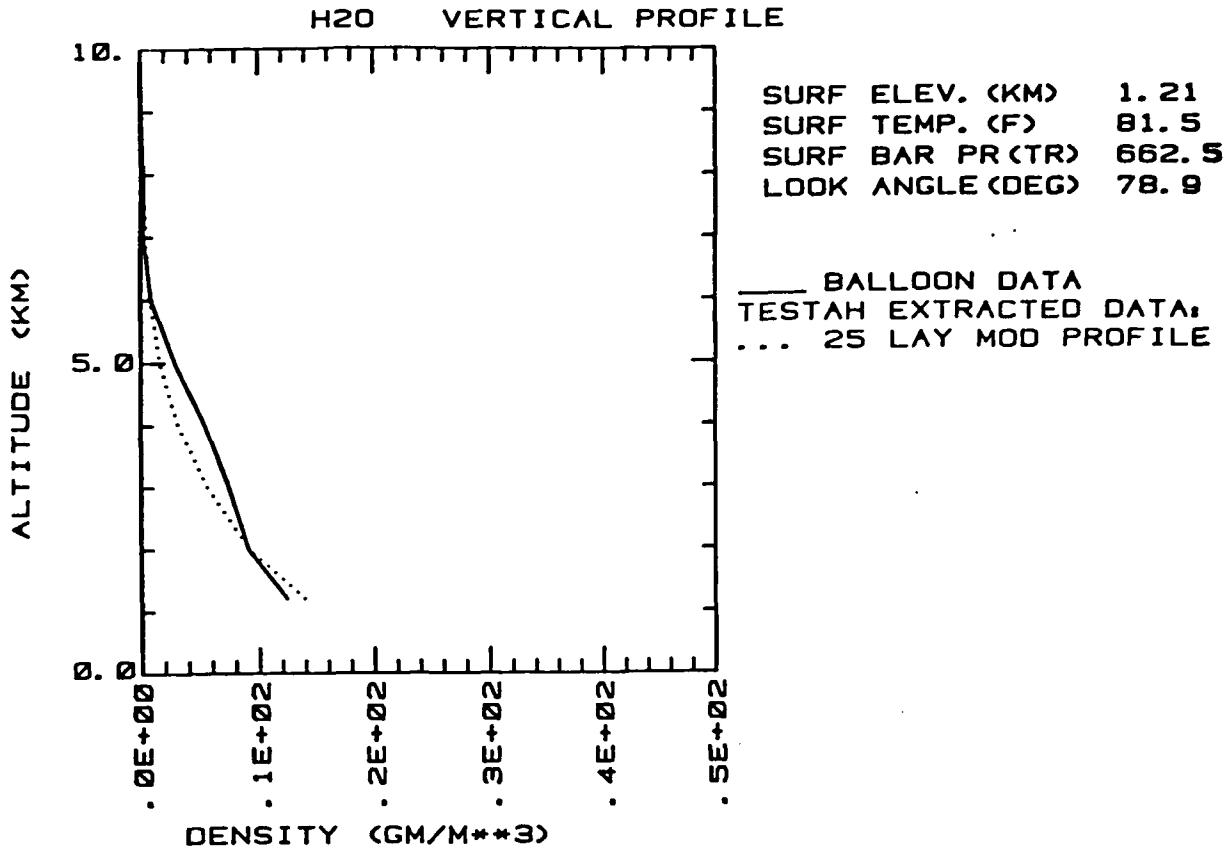

FIGURE 19b. THE H_2O VERTICAL DENSITY PROFILE RESULTING FROM THE BEST FIT SPECTRUM GIVEN IN FIGURE 18a IS SHOWN AS THE DOTTED CURVE. THE SOLID CURVE IS A BALLOON BORNE RADIOSONDE MEASUREMENT TAKEN THE SAME DAY IN THE MORNING.

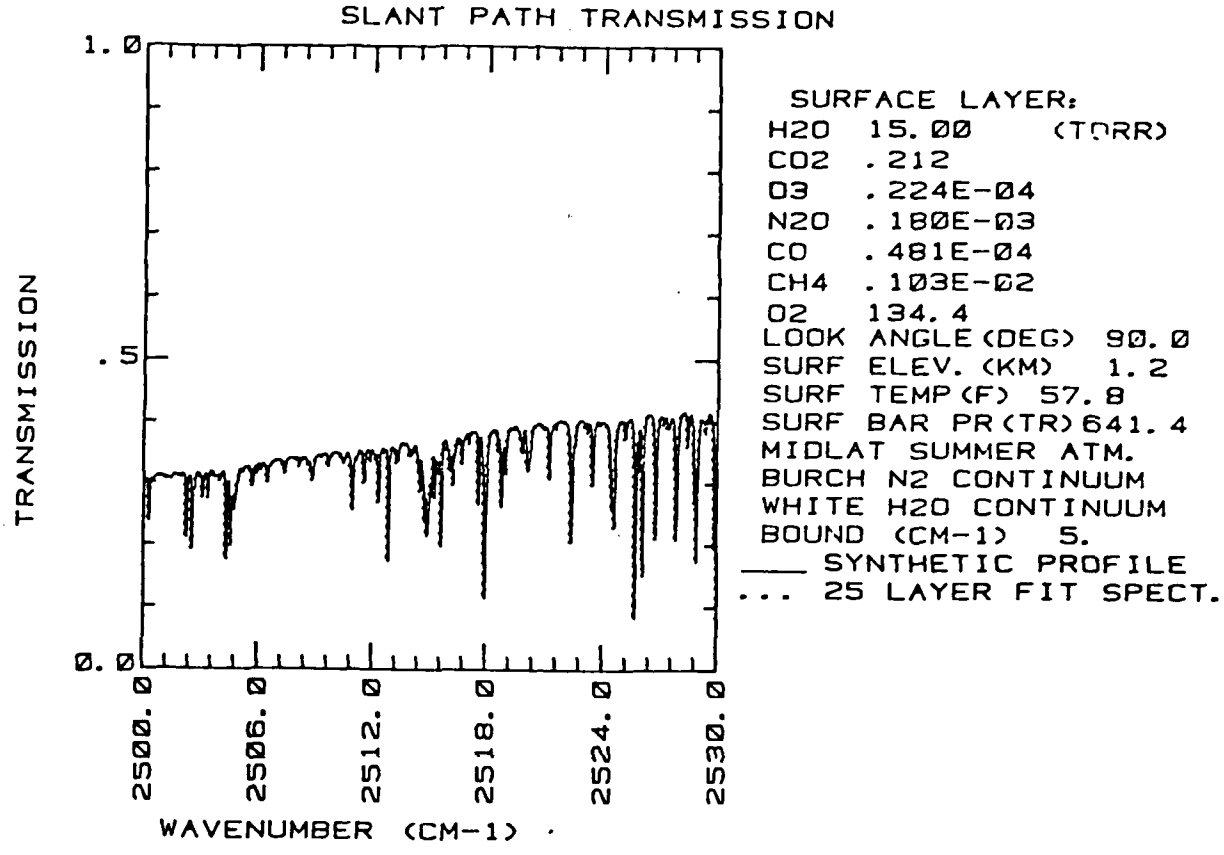

FIGURE 20a. THE SOLID CURVE IS THE SLANT PATH TRANSMISSION GENERATED BY A CHOSEN H_2O DENSITY VERSUS ALTITUDE PROFILE. THE DOTTED CURVE IS THE RESULT OF A 25 LAYER LEAST SQUARES FIT TO THE TRANSMISSION PROFILE (WITH NO KNOWLEDGE OF ASSUMED H_2O PROFILE).

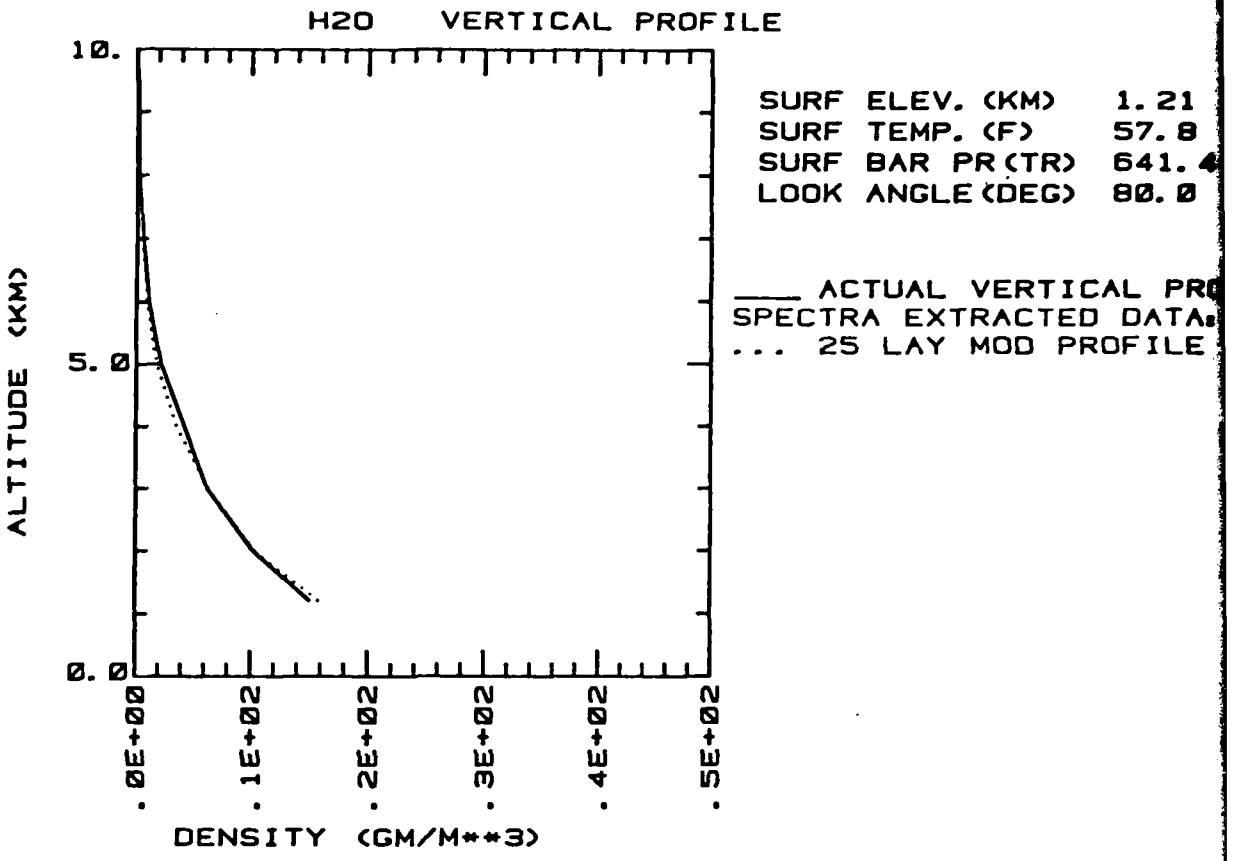

FIGURE 20b. THE SOLID CURVE IS THE ASSUMED H_2O DENSITY VERSUS ALTITUDE PROFILE. THE DOTTED CURVE IS THE H_2O DENSITY VERSUS ALTITUDE EXTRACTED BY THE 25 LAYER FIT ROUTINE BASED SOLELY ON THE TRANSMISSION SPECTRUM.

This test case is a very useful method for checking the validity of the procedure outlined above for extracting the vertical density profile of a particular molecular absorber. Since no noise is present in the "ideal" synthetic spectrum which contains a "known" vertical density distribution of the molecular absorber under study, and since no assumptions regarding the accuracy of spectral line parameters and continuum absorption coefficients are involved, the comparisons shown in Figure 20b tests the computational procedure alone, independent of the additional factors involed in extraction of profiles from the FTS data and comparisons to the balloon sonde data.

An improved fitting routine has been set up but not tested which will use the unique temperature of each layer as a discriminant of the distribution of the total burden of the molecule under study should be distributed. The uniqueness of the differing ground state energy levels and thermal populations for the various transitions is included in the molecular density distribution fitting procedure.

The calibrated solar spectra collected during the past two years provide a statistically significant data base of surface concentrations, vertical density profiles, and variations in the path integrated effects of the primary IR absorbing molecules and their isotopes. The most important one of these in the chemical laser region is HDO which is difficult to measure directly by means other than the Fourier Transform Spectroscopy used here.

3.3.3 FURTHER UTILIZATION OF EXISTING SLANT PATH FTS SOLAR SPECTRA

The problem of modeling long range detection of infrared target signatures can be addressed by use of FTS solar

spectra of low elevation angle paths. Transmission spectra at angles near 1^{o} above the horizon have been measured and provide useful data for long path detection analyses. Figure 9 shows an example of long path transmission and fair agreement with the model. The model computation for this case can be evaluated for the relative importance of the various absorption components at any specified frequency providing a better understanding of the problem.

Another application involving potential utilization of the slant path solar data is the detection and identification of trace and pollutant gases which absorb in the infrared. Information concerning abnormally high or low molecular concentrations and concentration fluctuations of the more abundant atmospheric molecules is also an important problem which can be addressed using the solar spectra.

4
CONCLUSIONS AND RECOMMENDATIONS

Upgraded FTS operating system software has been implemented on the system being used for slant path solar spectral measuements and tested as discussed in Sections 2.1 and 2.3. The new software allows increased spectral resolution to be used, facilitating critical comparisons of measured spectra to calculations of slant path atmospheric transmission. Certain modifications in data collection procedures were required to handle the larger data sets, but these have been satisfactorily accomplished so that the former data collection rate can be maintained.

The FTS system installation in the field measurement van has been completed allowing continued collection of slant path solar spectra to be carried out from a variety of measurement sites. In this way local influences peculiar to any of these sites may be studied. Although the major segment of the atmospheric slant path over which the transmission measurement is made is essentially independent of any particular location of the FTS system, the dominant influence of the atmospheric surface layer ($\sim$10 km) on absorbing gas composition and density allows "site peculiar" contributions to total absorption along the slant path to be studied.

Extinction coefficients at selected DF and CO_2 laser lines were derived from several examples of the FTS spectra and plotted against measured peak water vapor absorption coefficients for the H_2O line at 2844.01 cm^{-1} obtained from the same spectra. The results of these comparisons are shown in Figures 2 - 8. The correlation of the DF $P_3(12)$ and $P_3(7)$ line data (Figures 2 and 3) with measured

H_2O absorption coefficients is weak and relatively independent of increasing H_2O absorption, indicating the relative importance of extinction mechanisms other than water vapor at the frequencies of the two DF laser lines. Both of these lines are located in an N_2O absorption band. In addition the N_2 pressure-induced continuum absorption also contributes at these frequencies. By contrast the CO_2 laser line data shown in Figures 4 - 8 show good correlation with measured H_2O absorption coefficients demonstrating that water vapor absorption is the dominant extinction mechanism at these frequencies.

The slant path transmission model development described in Section 3.2 represents significant progress in the utilization of the slant path solar spectra collected during the past 2-1/2 years. Variability of a large number of modeling parameters may now be studied by comparing previously collected FTS data with the slant path model predictions. Improved understanding of ambient atmospheric gas compositions and their variability as well as identification of possible discrepancies in the AFGL line parameter listing should now be possible. Results of initial FTS-slant path modeling comparisons are shown in Figures 9 - 13 (Section 3.3.1). Initial indications based on these comparisons show that the 3 - 5 μm water vapor continuum absorption falls between the two competing models, at least for the atmospheric conditions encountered and for the spectral interval examined (2500 cm^{-1} to 2530 cm^{-1}). The above comparisons also point out disagreements between observed line strengths and computed values using the most current AFGL parameters for water vapor absorption lines near 2503 cm^{-1} and 2511 cm^{-1}. The comparison of FTS measurements to slant path calculations in the CO_2 laser region between 925 cm^{-1} and 955 cm^{-1} that is shown in Figure 14 indicates excellent agreement.

No modeling discrepancies are apparent in the data shown in Figure 14, however additional comparisons must be carried out before conclusive results can be obtained.

Use of the slant path modeling technique to extract vertical profiles of particular molecular absorbers is described in 3.3.2. The dominant atmospheric absorber, in the spectral region studied, namely water vapor is used as an example. The selection of test criteria and hierarchy of steps involved in the profile extraction procedures are illustrated by means of several examples shown in Figures 15 - 19. In these figures comparisons between vertical H_2O density profiles extracted from the FTS data to balloon sonde data are shown. Good results were obtained in the comparisons however certain limitations arise in the application of these techniques when pronounced temperature (and consequently water vapor density) inversions occur as a function of altitude.

A test of the uncertainty associated with the profile extraction procedure is described and results obtained in test calculations are presented in Figure 20. The test showed the ability of the extraction procedure to faithfully reproduce an H_2O profile which was used to calculate a synthetic test spectrum which was then substituted for an experimental slant path spectrum in the extraction procedure. Further development of this technique will be pursued since it establishes a procedure for using the FTS data in a "stand-alone" mode without the requirement for simultaneous atmospheric soundings for temperature, water vapor density, etc. As discussed in Section 3.3.2, uncertainties caused by atmospheric contamination from the balloon platform itself are avoided when the FTS spectra are used alone.

REFERENCES

1. B.L. Bean, W.L. Flowers, W.M. Gutman, A.V. Jelinek and R.L. Spellicy, Laser, IR and NMMW Propagation Measurements and Analyses, OptiMetrics, Inc. Report OMI-80-001, 1980.

2. W. Flowers, W. Gutman, Atmospheric Characterization Measurements at White Sands Missile Range: Point Sampling and Integrated Path Results, SAI Report SAI-79-002-AA, 1979.

3. W. Gutman, HEL Related Gas Analysis: Part II: Fourier Transform Solar Spectrum Measurements, SAI Report SAI-79-007-AA-II, 1979.

4. R.A. McClatchey, et al., AFCRL Atmospheric Absorption Line Parameters Compilation, Air Force Research Laboratories, L.H. Hanscom Field, Bedford, MA, AFCRL-TR-73-0096, 1973; L.S. Rothman, "Update of the AFGL Atmospheric Absorption Line Parameters Compilation", Appl. Opt. 17, 3517, 1978.

5. W.L. Wolfe and G.J. Zissis, The Infrared Handbook, IRIA, Environmental Research Institute of Michigan, 1978, Chapter 5.

6. F.S. Mills, Absorption of Deuterium Fluoride Laser Radiation by the Atmosphere, Ohio State Electro-Science Laboratory Report 4054-3, 1975.

7. J.E.A. Selby, E.P. Shettle and R.A. McClatchey, Atmospheric Transmittance from .25 to .28 μm: Supplement LOWTRAN 3B (1976), Air Force Geophysics Laboratory, Bedford, MA, AFGL-TR-76-0258, 1976.

8. R.E. Roberts, L.M. Biberman and J.E.A. Selby, Infrared Continuum Absorption of Atmospheric Water Vapor in the 8 - 12 μm Window, Paper P-1184, Institute for Defense Analyses, Arlington, VA, 1976.

9. W.R. Watkins and K.O. White, Water Vapor Continuum Absorption Measurements (3.5 - 4.0 μm) Using HDO Depleted Water, Optics Letters, 1, 31, (1977).

10. D.E. Burch, D.A. Grynak, and J.D. Pembrook, Investigation of the Infrared Radiation by Atmospheric Gases: Water, Nitrogen, Nitrous Oxide, Philco-Ford Aeronutronic Division Report U-4784, AFCRL-71-0124, 1974.

DISTRIBUTION LIST

6 COPIES

Commander/Director
Atmospheric Sciences Laboratory
Attn: DELAS-AS-P
Building 1622
White Sands Missile Range, New Mexico 88002